HOURGLASS SUBCYCLING APPROACH

HOURGLASS SUBCYCLING APPROACH FOR EXPLICIT TIME INTEGRATION OF FINITE ELEMENT

By

SHAN GAO, B.ENG.

A Thesis

Submitted to the School of Graduate Studies

in Partial Fulfillment of the Requirements

for the Degree

Master of Applied Science

McMaster University

September 2001

MASTER OF Applied Science (2001) McMaster University
(Mechanical Engineering) Hamilton, Ontario

TITLE: Hourglass subcycling approach for explicit time integration of finite elements

AUTHOR: Shan Gao, B.Eng.

SUPERVISOR: Dr. Don Metzger

NUMBER OF PAGES: xiii, 98

ABSTRACT

Explicit methods are widely used in finite element analysis as efficient ways to solve differential equations. The efficiency of explicit methods relies on the economical evaluation of internal forces at each time step. The greatest efficiency can be provided by one-point quadrature. However, instability arises because of the shortcomings in the use of one-point quadrature. The instability is called hourglass mode, or spurious singular mode. An effective method to control the instability is to add "hourglass stiffness" to an element integrated by one-point quadrature.

Explicit methods often require a very small time step to ensure stability. Thus, for complex problem with refined meshes, a very large number of timesteps will be required to complete the analysis. Minimizing the number of operations per time step can provide significant improvement on efficiency of the methods. Since hourglass terms typically require more computational operations than one-point quadrature terms, we are very interested in reducing the number of operations on hourglass control. In addition, considerable approximation is involved with hourglass control, and hence overall accuracy may not be seriously affected by relaxing the precision of the temporal integration of the hourglass force. Consequently, there is a possibility of trading some accuracy of the hourglass control for computational efficiency.

A subcycling approach is applied to the hourglass portion of explicit methods. Namely, instead of updating hourglass forces every time step, we update hourglass forces every two steps. The proposed approach is examined with the use of mass-spring models. The applicability to more complex models is demonstrated on a 3-D model with the subcycling approach implemented into an explicit finite element code. Efficiency, stability and accuracy are discussed as important issues of the proposed approach.

The mass-spring models and finite element implementation show that a beating instability can be introduced by the subcycling approach, and additional restriction is placed on the stable time step for the central difference operator. However, sufficient damping can restore the usual stability conditions. Thus, the proposed subcycling approach is seen to be highly advantageous where damping can be used, and it can cut computation time by 30% or more without significantly affecting the overall accuracy of the solution.

ACKNOWLEDGMENTS

I would like to express my sincere thanks to my supervisor Dr. Don Metzger for giving me the opportunity to work on this project and for his guidance, assistance and encouragement throughout the study.

TABLE OF CONTENTS

LIST OF FIGURES

LIST OF TABLES

PAGE

CHAPTER 1

INTRODUCTION

In this chapter, a brief overview of finite element method and background information of explicit method is presented. The proposed subcycling approach is introduced, and literature related to the approach is reviewed.

1.1 Finite element method

The finite element method, a numerical procedure for analyzing structures and continua, has become a very popular technique for the computer solution of complex problems in engineering. It originated as a method of stress analysis, and it was soon recognized that the method can be applied equally well to analyze problems of heat transfer, fluid flow, lubrication, electric and magnetic fields, and many others. Usually the problems addressed are too complicated to be solved satisfactorily by classical analytical methods.

The finite element procedure produces many simultaneous algebraic or ordinary differential equations, which are generated and solved on a digital computer. The development of the finite element method essentially began with the advent of digital

computer. Using the finite element method on a computer, it becomes possible to establish and solve many simultaneous governing equations for complex problems at reasonable cost. Today finite element procedures are used in the design of buildings, electric motors, heat engines, ships, airframes, and spacecraft. Finite element calculations can be performed on personal computers, mainframes, and all sizes in between [1].

The finite element method is most widely used for structural mechanics. When applied to structural mechanics problems, the finite element method generally idealizes the total structure as an assemblage of small elements that are interconnected at the structural joints. Each element is of simple geometry and therefore is much easier to analyze than the actual structure [1]. The element stiffness matrices are calculated and the total stiffness matrix is formed by the addition of the element stiffness matrices. The known loads are applied and how the structure is supported is specified. The solution of the equilibrium equations of the assemblage of elements yields the modal displacements, which are then used to interpolate the displacement field and calculate the element stresses. Finally, the element displacements and stresses must be interpreted as an estimate of the actual structural behavior [2].

In essence, the finite element method approximates a complicated solution by a model that consists of piecewise-continuous simple solutions. Elements are called "finite" to distinguish them from differential elements used in Calculus. The power of the finite element method resides principally in its versatility. The method can be applied to

various physical problems. The body analyzed can have arbitrary shape, loads, and support conditions. The mesh can mix elements of different types, shapes, and physical properties. Another attractive feature of finite element method is the close physical resemblance between the actual structure and its finite element model. The model is not simply an abstraction. This is especially true in structural mechanics [1].

Results of finite element analyses are rarely exact. However, errors are reduced by using more elements and processing more equations, and results accurate enough for engineering purposes are obtainable at reasonable cost [1].

1.2 Computational efficiency

In practical analysis, the proper idealization of the actual problem is very important. A few good elements may produce better results than many poorer elements. However, in general, the accuracy of the analysis can be improved if a more refined finite element mesh is used. Therefore, an analyst may tend to employ very large finite element systems to approximate the actual structure. In large-scale finite element analyses, thousands of elements and large computational effort are required.

In finite element analysis, the time for solution of the equilibrium equations can be a large percentage of the total solution time. Thus, the overall efficiency of a finite element analysis depends to a large degree on the numerical procedures used for the

solution of the system equilibrium equations. If inappropriate algorithms are used, the total cost of analysis is affected a great deal, and indeed the cost may be many times larger than is necessary.

Much research effort has been made to optimize the numerical procedures for the solution of the equilibrium equations. In the early use of the finite element method, systems of equations of the order 100 were considered to be large, while currently equations of the order 10,000-100,000 are solved without much difficulty. Still, there is a lot of room and incentive for reducing the computational expense and getting the results faster, as hundreds of millions of dollars are spent each year on finite element modeling and computer costs.

Explicit Methods are one commonly used class of algorithms for the solution of equilibrium equations in dynamic analysis. In this thesis, the objective is to improve the computational efficiency of the Explicit Method based on the central difference operator.

1.3 Explicit Method

Explicit methods and implicit methods are two categories of direct integration. The basic concept of explicit methods and direct integration can be explained as following.

Derived by requiring the work of external forces to be absorbed by the work of internal, inertial, and viscous forces, equations that govern the dynamic response of a system of finite elements can be written in the form

$$M\ddot{U}+C\dot{U}+KU=R \qquad (1.1)$$

where M, C, and K are the mass, damping, and stiffness matrices; R is the external force vector; and $\ddot{U},\dot{U}$, and U are the acceleration, velocity and displacement vectors of the finite element assemblage.

Equation (1.1) represents a system of ordinary differential equations of second order. In principle, the solution to the equations can be obtained by standard procedures for the solution of differential equations. However, the procedures proposed for the solution of general systems of differential equations can be very expensive if the order of the matrices is large. Therefore, in practical finite element analysis, a few effective methods are applied. Generally, the procedures commonly used can be divided into two methods of solution: direct integration and mode superposition. The two techniques are closely related, and the choice for one method or the other is strongly problem-dependent. For many structural dynamics problems, direct integration is more expedient.

In direct integration, the equations in (1.1) are integrated using a numerical step-by-step procedure. The approach is to satisfy the equation (1.1) only at discrete time intervals, instead of trying to satisfy the equation (1.1) at any time step,

$$M\ddot{U}_n + C\dot{U}_n + KU_n = R_n \qquad (1.2)$$

where subscript n denotes time $n\,\Delta t$, and Δt is the time step.

In the procedure, the time span under consideration, T, is divided into N equal time intervals Δt ($\Delta t = T/N$). Assuming that the displacement, velocity and acceleration vectors at time 0 are known, the integration scheme calculates approximate solutions at times $\Delta t, 2\Delta t, \ldots, T-\Delta t, T$.

A popular integration scheme is the central difference method. It assumes that

$$\ddot{U}_n = \frac{1}{\Delta t^2}\{U_{n+1} - 2U_n + U_{n-1}\} \qquad (1.3)$$

and

$$\dot{U}_n = \frac{1}{2\Delta t}\{U_{n+1} - U_{n-1}\} \qquad (1.4)$$

Combining equations (1.3) and (1.4) with (1.2), we obtain

$$(\frac{1}{\Delta t^2}M + \frac{1}{2\Delta t}C)U_{n+1} = R_n - (K - \frac{2}{\Delta t^2}M)U_n - (\frac{1}{\Delta t^2}M - \frac{1}{2\Delta t}C)U_{n-1} \qquad (1.5)$$

from which we can solve for U_{n+1}.

In the procedure, U_{n+1} is calculated in terms of completely historical information of the equilibrium conditions at time $n\Delta t$ and before. For this reason, the integration procedure is called an Explicit Integration Method or Explicit Method.

On the other hand, the Newmark [27], Houbolt [28], and Wilson methods [29], require knowledge of the time derivatives of U_{n+1}, which are unknown. Thus, those methods are called Implicit Integration Methods.

Using the explicit method, such as the central difference method, can save computational efforts. However, it becomes unstable when the time step is too large.

1.4 Time Step

The central-difference method, as well as explicit methods in general, is conditionally stable. If time step Δt is too large, the method fails. For equation (1.5) to be conditionally stable, the time step Δt is required to be smaller than a critical value

$$\Delta t \leq \Delta t_{cr} = 2/\omega_{\max} \qquad (1.6)$$

where $\omega_{\max}$ is the highest natural frequency of the finite element system [1]. If the time step is larger than Δt_{cr}, the computations will be unstable as errors resulting from the integration or round-off in the computer grow and make the response calculations worthless.

The natural frequency, $\omega_{\max}$ can be obtained by determining the eigenvalues λ that satisfy

$$\det[\, K - \lambda M \,] = 0\,, \quad \text{where } \lambda = \omega^2 \qquad (1.7)$$

If the smallest diagonal element of the mass matrix is very small, the largest eigenvalue λ_{max} of equation (1.7) and ω_{max} will become very large. Correspondingly, the time step Δt will have to be very small. As a result, for refined meshes with small element size, the integration will require a very large number of timesteps N ($N=T/\Delta t$) to complete an analysis.

Reducing the number of operations per time step is of great importance in order to maintain the practicality of the method.

1.5 One-point Quadrature

The derivation of the finite element stiffness matrix and element load vector requires integration over a line, area or volume. For high-order elements, the integral expressions are very lengthy and complex. Accordingly, to reduce the number of operations, integration is done numerically instead, usually by schemes known as Gauss quadrature. The basic concept of Gauss quadrature can be explained with the example of one-point quadrature.

With the substitution

$$\chi = \frac{1}{2}(1-\xi)\chi_1 + \frac{1}{2}(1+\xi)\chi_2 \qquad (1.8)$$

we can transform

$$I = \int_{x_1}^{x_2} f(x)dx \qquad (1.9)$$

into

$$I = \int_{-1}^{1} \phi d\xi . \qquad (1.10)$$

The integrand $f = f(x)$ is changed into $\phi = \phi(\xi)$. After the transformation, we can approximate the integral in a simple way, evaluating ϕ at the midpoint $\xi = 0$ and multiplying by the length of the interval. Thus, in essence, the area under curve is approximated by a rectangular area of height $\phi(0)$ and length 2, so that $I = 2\phi(0)$ (Fig. 1.1). This is called one-point Gauss quadrature rule.

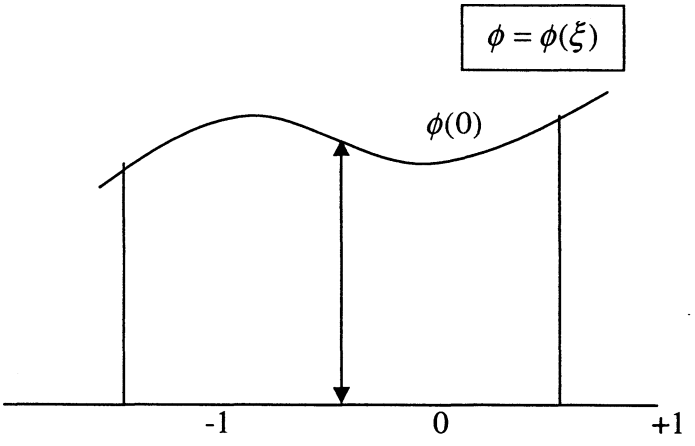

Figure 1.1 Gauss quadrature using one sampling point

The foregoing procedure can be extended into n-point Gauss quadrature (1.11)

$$I = \int_{-1}^{1} \phi d\xi \approx W_1\phi_1 + W_2\phi_2 + \Lambda + W_n\phi_n \qquad (1.11)$$

Thus, to approximate I, we evaluate $\phi = \phi(\xi)$ at each of sampling points ξ_i to obtain ordinates ϕ_i, multiply each ϕ_i by an appropriate weight W_i, and add. Figure 1.2 shows the example of three sampling points. In the one-point example, we have $n = 1$ and $W_i = 2$.

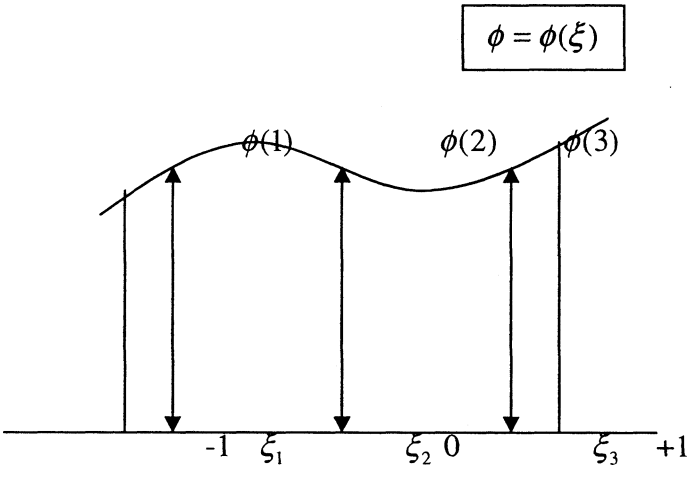

Figure 1.2 Gauss quadrature using three sampling points

Gauss was able to prescribe the sampling points ξ_i and weights W_i such that greatest accuracy is achieved for a given n. Generally, as more points are used, Gauss quadrature becomes more accurate. For numerically integrated elements, a quadrature rule sufficient to provide the exact integrals of all terms in the element stiffness matrix is considered "full integration". But full integration also requires more computational effort. Since the expense of generating a matrix [k] by numerical integration is proportional to the number of sampling points, using more sampling points means higher cost. Moreover, full integration involves difficulties such as volumetric locking for incompressible

materials and shear locking for bending-dominated problems. Thus, a lower-order quadrature rule, called "reduced integration", may be desirable for saving computational efforts and softening an element, thus countering the overly stiff behavior associated with full integration.

Two-dimensional and three-dimensional Gauss quadrature rules can be formed by successive application of one-dimensional Gauss rules.

Gauss quadrature schemes can be applied to form the stiffness matrices and evaluate internal forces. Note that internal forces must be calculated at each time step. It is the most expensive part of the per-time-step cost of the explicit method. Hence, there is considerable incentive to use one-point quadrature to evaluate internal forces. For instance, explicit transient analysis with the four-node bilinear quadrilateral element with one-point quadrature is expected to be roughly one-fourth as expensive as analysis using four-point quadrature. Special programming techniques make one-point quadrature more efficient, and in three dimensions, the savings are even more dramatic.

Using one-point quadrature schemes to form the stiffness matrices and force vectors provides tremendous benefits because the number of evaluations of the material constitutive law is reduced substantially. However, one-point quadrature scheme also has disadvantages.

1.6 Hourglass Mode

The major drawback of one-point quadrature rule is that a so-called hourglass instability arises.

When stiffness matrix K is calculated by a one-point quadrature rule, it contains only the information that can be sensed at the sampling points. If it happens that strains are zero at all sampling points for a certain deformation mode, then stiffness matrix K will exhibit zero-stiffness in the sense that strain energy is zero for this particular element response. In effect, the matrices are singular with respect to a number of displacement patterns other than the rigid body patterns. The use of a one-point quadrature scheme results in certain deformation modes remaining stressless. If a mesh is consistent with a global pattern of these modes, the deformation will grow unresisted by internal force to destroy the solution.

These modes are also called spurious singular modes, kinematic modes, or zero-energy modes. The term "zero-energy mode" refers to a nodal displacement vector that is not a rigid-body motion but nevertheless produces zero strain energy. We expect that strain energy is zero if a nodal displacement vector is a rigid-body motion. If strain energy is zero when a nodal displacement vector is not a rigid-body motion, then an instability is present. These modes can appear in a mesh of elements as well as in a single element. For example, two dimensional four-node quadrilateral element possesses two

such modes (Figure 1.3). The mechanisms are called hourglass modes because of their shape.

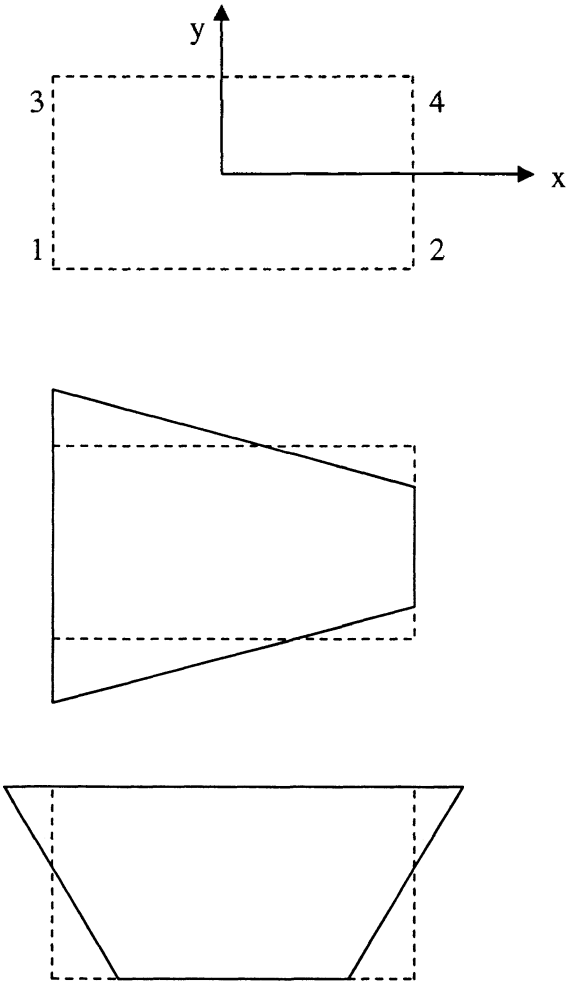

Figure 1.3 Hourglass modes

Therefore, when one-point quadrature is used to evaluate element integrals, the hourglass modes must be controlled if useful results are to be obtained.

1.7 Hourglass Control

Various hourglass control methods have been proposed. Their goal is to eliminate instability by providing restraint.

An effective way to control hourglass instabilities is to add "hourglass stiffness" to an element integrated by one-point quadrature. This can be written in the form

$$K = K_0 + K_{hg} \tag{1.12}$$

where K_0 is the one-point quadrature stiffness and K_{hg} is the hourglass stiffness [7].

Typically, the methods of determining K_{hg} require more operations than the one-point quadrature part of the element formulation. Thus, we are more interested in reducing the number of operations in the hourglass part of the problem.

In addition, since considerable approximation over the quadrature is involved in practical hourglass control, the accuracy of the hourglass part of the formulation is not so important as long as the stabilizing forces control hourglass modes. Consequently, sacrificing some accuracy of the hourglass control could provide significant efficiencies without seriously affecting the accuracy of the analysis.

1.8 Subcycled Hourglass Control

In this thesis, basically a subcycling approach is applied to the hourglass part of the problem. Subcycling is generally applied by subdividing the spatial domain into several regions. The smallest elements will be updated each step, while larger elements may be updated every N steps.

Here, the concept of subcycling involves a different way of subdiving the model. Instead of dividing the geometry spatially, the model is split into exactly two parts, one-point quadrature and hourglass control. The one-point quadrature component is updated each time step, and the hourglass control component is updated every other step. The subcycled hourglass control approach could provide improved computational efficiency by saving expensive hourglass force calculation.

The proposed approach is explored in detail with the use of one, two and more degree of freedom mass-spring analogies. Applicability to more complex models is demonstrated on a 3-dimensional finite element example. The goal of the subcycling method is to gain computational efficiency. However, it should be realized that stability must be assured, since otherwise the errors grow and make the response calculations worthless in most cases. Thus, stability is examined in detail, while the overall accuracy is considered.

1.9 Literature Review

In finite element analysis, full integration has been widely used because good convergence and stability are always achieved; however, full integration requires many computational efforts to construct an element stiffness matrix and internal force vector. In large-scale analysis with thousands of elements, the computational cost can be very high. Furthermore, the fully integrated continuum tends to lock if the behavior of the material becomes incompressible or nearly incompressible. A remedy for this is to use the selective reduced integration in which the full quadrature and the reduced quadrature are applied to different terms to form the element as proposed by Malkus and Hughes [3] and Nagtegaal et al., [4] among others. However, it is as costly as full quadrature.

The one-point quadrature is the most efficient to evaluate an element stiffness matrix, but suffers instabilities such as the hourglass modes in certain cases. These were first recognized in the finite difference literature [5]. They are a special case of the phenomenon known in finite elements as zero-energy modes. In static solutions, they lead to singularity of the stiffness matrix for certain boundary conditions.

Numerous techniques have been developed for the control of the hourglass modes in the four node quadrilateral and the corresponding two-dimensional finite difference equations used in Lagrangian finite differences codes. One of the earliest of these is the technique developed by Maenchen and Sack [5] who added artificial viscosity to inhibit

opposing rotations of the sides of the quadrilateral zone. The finite element versions of the Maenchen and Sack anti-hourglass viscosity have been developed by Belytschko and Kennedy [6], Flanagan and Belytschko [7], and Belytschko et al [8].

In those methods, the main process of hourglass control has been constructed by introducing parameters for "artificial damping" and "artificial stiffness". The anti-hourglass mode vectors γ which are derived by orthogonal conditions play an important role in the construction of a stabilization stiffness matrix and an additional correction force vector to avoid hourglass phenomena.

An alternative approach for hourglass control, the uniform reduced integration scheme, was proposed by Liu et al. [9, 10] in which the resulting stabilization matrix requires no stabilization parameter. It is shown that the stabilization vector γ can be obtained simply by taking the partial derivatives of the generalized strain vector with respect to the natural co-ordinates. The strain vector is therefore approximated by the combination of a constant part and other parts involving strain derivatives. In the papers, a more complete mathematical formulation of a unified hourglass control was formed, and a thorough interpretation relating the results to full quadrature elements is given. However, the implementation and application of the theory is only presented for 2-D elements and linear problems. Metzger and Sauve [11] presented a 3-D application of the unified theory, using a more appropriate rate formulation for nonlinear elastic-plastic problems.

Koh and Kikuchi have proposed a so-called directional reduced integration approach [12] in which the anti-hourglass gradient matrix is derived analytically and is projected to eliminate various hourglass modes including the special torsional hourglass modes in 3-D state. In contrast to selective reduced integration, where certain parts of internal virtual work are underintegrated uniformly in all directions, the directional reduced integration underintegrates in certain directions. Numerical examples show that this technique is effective for two-dimensional problems. However, directional reduced integration cannot always keep the correct rank of the stiffness matrix.

Liu and Belytschko et al. [13] proposed a new simple approach which is called a multi-point quadrature scheme or selective integration scheme, in which two point quadrature was used for 4-node quadrilateral element in elastoplastic dynamic analysis by explicit interation time scheme. The main advantage of this approach is that the implementation is easier and the results may be more accurate for plasticity calculations than those for uniform reduced integration scheme.

Lately, it was realized that the earlier approach by Belytschko and coworkers [8] leads to locking for incompressible materials in plane strain. In the scheme, the stabilization does not project out volumetric strains, so for incompressible materials it is possible for the element to become quite stiff or even lock as the stabilization parameter is increased. This is particularly important in the nonlinear range where many materials are almost incompressible. The earlier implementation of hourglass control were

improved by Belytschko and Bindeman [14, 15]. A stabilization based on the Simo-Hughes assumed strain method is developed. The assumed strain fields are constructed so that those portions of the fields which lead to volumetric and shear locking are eliminated by projection. The stabilization forces depend only on the element geometry and material properties. User specified parameters are not needed.

All the approaches mentioned above strive to minimize the computational effort. Typically, an effective method requires more operations for the hourglass terms than for the one point quadrature part of the element formulation. This is true for the early method of Flannagan and Belytschko [7], Belytschko et al. [8]. The approach proposed by Lui et al. [9, 10] and Belytschko [14, 15] provide more sound hourglass correction terms, but require even more operations. A more simple, approximate method implemented by Metzger and Sauve [11] still requires about twice as many operations for the hourglass calculation as for the one point quadrature part of the formulation. Therefore, in order to improve the overall computational efficiency of the analysis, special care should be given to the hourglass part of the formulation.

Another feature of those hourglass control methods is that the accuracy of the hourglass part of the formulation is not so important as long as the stabilizing forces control spurious motions. Thus, the precision of the temporal integration of the hourglass force may be relaxed without seriously affecting the accuracy of the analysis.

Based on the two features of the hourglass control schemes, evaluating the hourglass terms on a larger time interval could be highly advantageous, as long as a tractable scheme can be established.

1.10 Objective

In this thesis, the objective is to explore the possibility of evaluating the hourglass terms every other step, which could provide Explicit Method with significant efficiencies. This is basically a subcycling approach applied to the hourglass portion of the problem. Among the issues of the proposed subcycling approach are efficiency, stability and accuracy.

CHAPTER 2

METHODOLOGY

In this chapter, mass-spring analogy of the hourglass control is established. The algorithm shows how the concept of subcycling is applied to the hourglass part of the problem.

2.1 Mass-spring Model of Hourglass Control

The mass-spring model is useful in understanding the hourglass control equation

$$K = K_0 + K_{hg}$$

Mass-spring model is simple and easy to test, and applies the same concept of finite element method. A one degree of freedom model represents single-element finite element model, while higher degree of freedom models represent finite element models with more elements.

The stiffness matrix K_0 can be regarded as a generalized network of springs, and the hourglass stiffness K_{hg} can be regarded as additional parallel springs. A simple model shown in Figure 2.1, has a one degree of freedom mass attached to a spring representing the one-point quadrature stiffness. Another spring, representing the hourglass stiffness, is

connected in parallel to the same mass. The dimensionless parameter, b, relates the one-point stiffness and the hourglass stiffness.

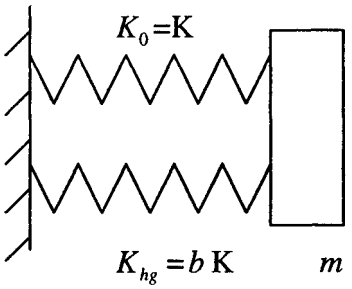

Figure 2.1 One degree of freedom mass-spring model

The mass-spring analogy above provides an easy and understandable way to study the response of the subcycling approach.

2.2 Subcycling

In explicit method, the maximum time step is limited by the maximum natural frequency of a finite element

$$\Delta t \leq \Delta t_{cr} = 2/\omega_{\max} \qquad (1.6)$$

In many finite element models that are composed of non-uniform meshes, a group of small elements may require a much smaller time step than the stable time step for the rest of the elements. If only one time step is used, the computation needed to solve the problem will be increased significantly. For example, in Figure 2.2, because of the presence of smaller elements the mesh on the left is much more expensive than the mesh on the right [17].

Subcycling, which uses different time steps in different portions of the meshes, has been developed by Belytschko, Yen, and Mullen [18]. It is also called multi-time-step integration. The idea behind subcycling is to sort elements based on their size into groups whose step size is some even multiple of the smallest element step size, $2^{(n-1)}\Delta t$, for integer values of n greater than or equal to 1 [17]. The group with the smallest elements will be updated each step, while other groups may be updated every $2^{(n-1)}$ steps.

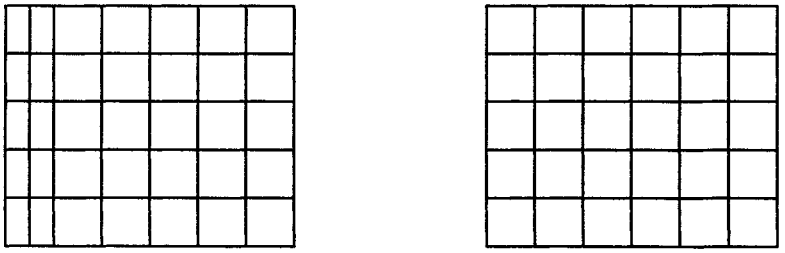

Figure 2.2 The left mesh is much more expensive to compute than the right

Subcycling eliminates the need to update the entire mesh with the stable time step of the smallest elements in the mesh, significantly reducing the computation needed to solve the problem. Thus, subcycling is of considerable value in the explicit integration of many engineering problems in which non-uniform meshes are needed.

However, when a problem is dominated by a large number of small elements, this subcycling approach provides minimal improvement. Another major difficulty of this subcycling approach lies in how elements along the interface between large and small elements are handled, a subject that is beyond the scope of this thesis.

In this thesis, the concept of subcycling is applied to the integration, rather than to a spatial subdivision of the geometry. Thus, the problem of dealing with the interface between large and small elements is not encountered. The integration is split into exactly two parts. The first part is the one-point quadrature component, which is updated every time step. The second part is the hourglass control component, which is to be updated every other time step. This can greatly save computational effort on the hourglass terms.

On the basis of the mass-spring analogy for a structural model, the subcycling approach represents subdivision of the model into parallel connected submodels, while the usual approach represents subdivision of the model into submodels connected in series. Either way, the implementation is straightforward in any explicit code once the subdivision is established [16].

2.3 Subcycling Algorithm

For the mass-spring model, the equation of motion is to be integrated with the central difference method. However, as the subcycling method applies to the hourglass control, the internal force in the hourglass spring is to be updated only on even steps. As shown in Table 2.1, on odd steps, the increment in hourglass force is set to zero, so that the previous hourglass force is retained. The only change from the normal central difference method is step 2, where the hourglass force increment is calculated [16].

1. Initial conditions: $U_0, \dot{U}_{-\frac{1}{2}}$

2. Determine force increment:

$$\dot{F}_0^{n-1/2} = K_0 \dot{U}_{n-1/2},$$

$$\dot{F}_{hg}^{n-1/2} = K_{hg} \dot{U}_{n-1/2}, \qquad \text{n even}$$

$$\dot{F}_{hg}^{n-1/2} = 0 \qquad , \qquad \text{n odd}$$

3. Update force and calculate acceleration

$$F_{\text{int}}^n = F_{\text{int}}^{n-1} + \Delta t \dot{F}_0^{n-1/2} + \Delta t \dot{F}_{hg}^{n-1/2}$$

$$\ddot{U}_n = M^{-1}(F_{ext}^n - F_{\text{int}}^n)$$

4. Update velocity and displacement

$$\dot{U}_{n+1/2} = \dot{U}_{n-1/2} + \Delta t \ddot{U}$$

$$U_{n+1} = U_n + \Delta t \dot{U}_{n-1/2}$$

5. Repeat steps 2-4 to the end of analysis

Table 2.1 Subcycling algorithm

2.4 Discussion

The mass-spring model can be extended into N degree of freedom models. The subcycling algorithm is applicable for those models, while corresponding matrices are used. For a practical problem with thousands of degrees of freedom, it can be expected that the expensive hourglass force calculation would be avoided 50% of the time as long as stability and accuracy are ensured. In the following chapters, stability and accuracy of the proposed approach are examined.

CHAPTER 3

STABILITY

In order to gain computational efficiency with the subcycling method, additional stability conditions must not negate the savings of the less frequent hourglass force updates. Thus, stability behavior of the subcycled hourglass control model is of great interest. In this chapter, several mass-spring models with different numbers of degrees of freedom are used to study the stability of the subcycling approach.

3.1 Introduction

The stability of the central difference operator with subcycled hourglass control cannot be analyzed with the usual difference equation approach. Thus, the stability behavior of the subcycling approach is established with a numerical study.

For the normal central difference operator to be stable, the time step is required to be smaller than the critical time step

$$\Delta t \leq \Delta t_{cr} = 2/\omega_{\max}$$

Thus, stability and time step are inseparably linked. Time step ratio, TSR, defined as

$$TSR = \frac{\Delta t}{\Delta t_{cr}} \tag{3.1}$$

is a useful definition of the relative size of the time step used in direct integration [1]. In the study, the relationship between time step ratio and stability is closely examined.

Another factor that needs to be considered is the magnitude of the hourglass stiffness. This is easy to understand. If the hourglass force is significant in the integration, skipping some of the evaluation of the hourglass forces is more likely to incur instability. Therefore, stability is also affected by the parameter b, which relates the one-point stiffness and hourglass stiffness.

Generally, for certain combinations of TSR and b, the subcycled hourglass control approach becomes unstable. Our objective here is to find the pattern, or so-called stability map. In this section, stability maps of different degree of freedom models are established with respect to TSR and b.

3.2 Bisection Method

A bisection method is applied in finding the stability maps of the models. The concept of bisection is generally used for finding the estimate of the root of the equation $f(x) = 0$. In general, if $f(x)$ is real and continuous in the interval from x_l to x_u, and $f(x_l)$ and $f(x_u)$ have opposite signs, then there is at least one real root between x_l and

x_u. We pick the midpoint x_m (bisect the interval) and evaluate the function there. If $f(x_1)f(x_m) < 0$, then there is a sign change in (x_1, x_m); if $f(x_1)f(x_m) > 0$, then there is a sign change in (x_m, x_u); if $f(x_1)f(x_m) = 0$, then x_m is a root. Repeated bisections reduce the interval containing the sign change to an arbitrarily small length. Thus, the method could be continued to obtain a refined estimate of the root, which meets the prespecified criterion.

In this thesis, the concept of bisection is used to find the boundary of the unstable region. For example, in Figure 3.1, for a certain parameter b, the system may be stable with TSR_1, but unstable with TSR_2, then there must be at least one boundary of the unstable region between TSR_1 and TSR_2. We set up an indicator of stability, IS, which is 1 when the system is stable and –1 when the system is unstable. Then stability behavior of the system with the midpoint TSR_m is evaluated. If IS(TSR_1)IS(TSR_m) = -1, then the boundary is between TSR_1 and TSR_m; if IS(TSR_1)IS(TSR_m) = 1, then the boundary is between TSR_m and TSR_2.

In Figure 3.1, we have IS(TSR_1) = 1 and IS(TSR_m) = 1, therefore the boundary is between TSR_m and TSR_2. We evaluate the stability behavior with the midpoint TSR_m^2 between TSR_m and TSR_2, and get IS(TSR_m^2) = -1. Thus, the boundary is between TSR_m^2 and TSR_m. Then the midpoint between TSR_m^2 and TSR_m will be evaluated. Notice

that the interval containing the boundary is reduced with every bisection step. This gives us refined estimates of the location of the boundary. The process can be repeated until the estimate is as accurate as the prespecified acceptable level.

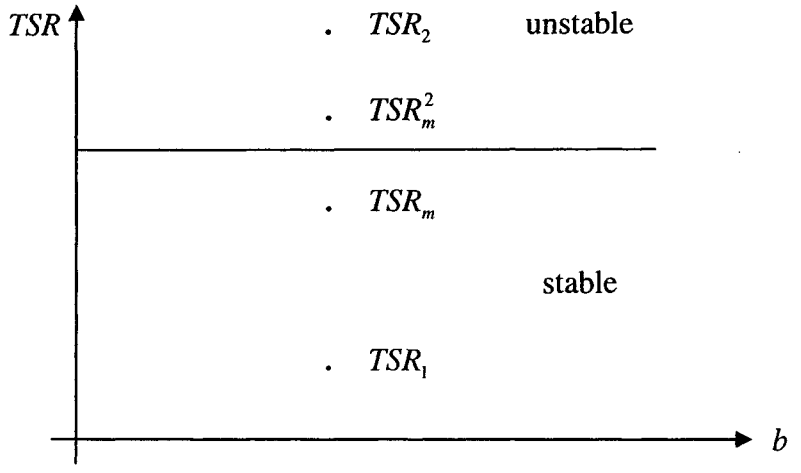

Figure 3.1 Use of bisection method to find the unstable region

Notice also that the boundary of unstable region is not necessarily horizontal. Therefore, we need to use the bisection method for different values of parameter b. A simple algorithm for the bisection method is listed in Table 3.1.

The difficulty of the bisection method lies in choosing the proper initial guess points, TSR_1 and TSR_2, because there may be multiple boundaries of unstable regions between TSR_1 and TSR_2. The approach to this problem is presented later in the section.

1. For a certain value of b, choose lower guess point TSR_1 and upper guess point TSR_2 such that there is a boundary of unstable region over the interval. This can be checked by ensuring that IS(TSR_1)IS(TSR_2) = -1.

2. An estimate of the location of boundary is determined by

$$TSR_m = (TSR_1 + TSR_2)/2$$

3. Make the following evaluations to determine in which interval the boundary lies:

   (a) If IS(TSR_1)IS(TSR_m) = -1, the boundary lies in the lower subinterval. Therefore, set $TSR_2 = TSR_m$ and return to step 2.

   (b) If IS(TSR_1)IS(TSR_m) = 1, the boundary lies in the upper subinterval. Therefore, set $TSR_1 = TSR_m$ and return to step 2.

4. Repeat steps 2-3 until $|TSR_1 - TSR_m| <$ EPS, where EPS is the stopping criterion.

5. For a different value of parameter b, repeat steps 1-4.

Table 3.1 Algorithm for the bisection method

3.3 One degree of freedom model

One degree of freedom model provides us with basic understanding of the stability behavior of the subcycled hourglass control approach.

As for the one degree mass-spring model, the time step ratio TSR, is based on the total stiffness and mass so that

$$TSR = \frac{\Delta t}{\Delta t_{cr}} = \frac{\Delta t}{2}\sqrt{\frac{k_0 + k_{hg}}{m}} \qquad (3.2)$$

Examination of this model reveals that the stability behavior is identical for all modes when normalized according to their respective frequencies. Thus, for the model shown previously in Figure 2.1, we normalize it by choosing K and m with identical value. The frequency of the system will be determined by parameter b. Therefore, equation 3.2 can be written as

$$TSR = \frac{\Delta t}{2}\sqrt{1+b} \qquad (3.3)$$

An unusual relationship between instability and the time step ratio is encountered in the numerical study. If the hourglass stiffness has a small value and the time step ratio is near $1/\sqrt{2}$, a beating process arises between two close frequencies. A normal one degree of freedom model has only one frequency, but here another frequency arises because of the subcycled approach. Detailed explanation on this subject is beyond the

scope of this thesis. Figure 3.1 shows an example of the beating of one degree of freedom model with parameter b =0.6 and TSR =0.707.

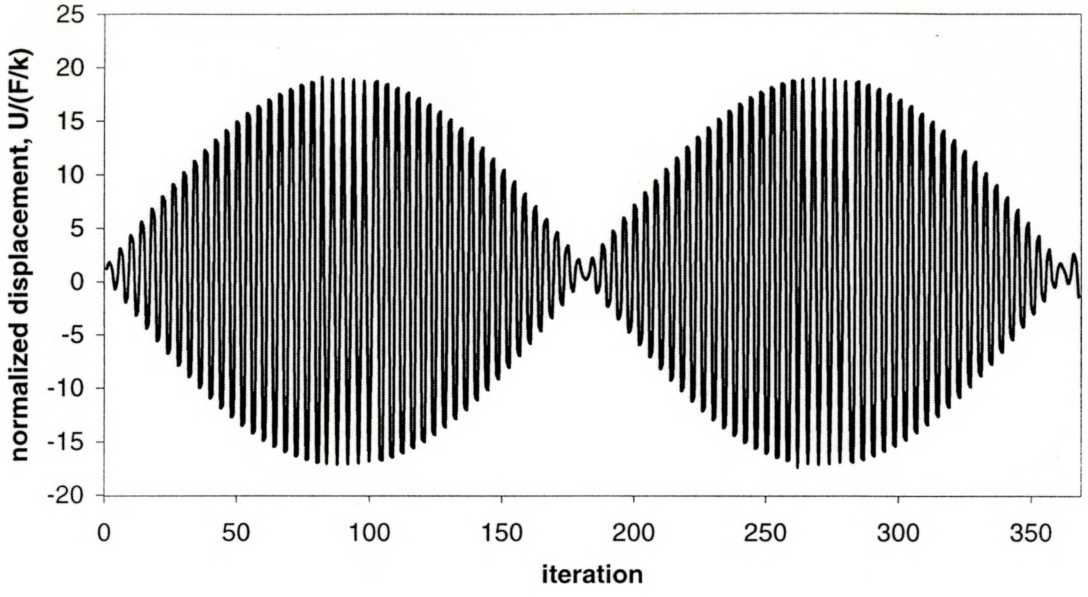

Figure 3.2 Beating of mass-spring model with b =0.6, TSR = 0.707

As TSR becomes larger than $1/\sqrt{2}$, the beating process grows into instability. However, when TSR is larger than a certain value and smaller than 1, the system becomes stable again. This is shown in Figure 3.3. The upper boundary of the unstable region is determined by bisection method. It is not difficult to choose initial guess points, TSR_1 and TSR_2, because there is only one unstable region. The lower boundary is TSR = $1/\sqrt{2}$ where the beating occurs. The instability starts from the extreme left point, where parameter b is approaching zero. As b becomes larger, representing larger value of hourglass stiffness, the point spreads to form a band of finite width. This confirms the

stability behavior that we expect. Notice that b is between 0 and 1, because the hourglass stiffness is never larger than the primary stiffness for practical hourglass control methods.

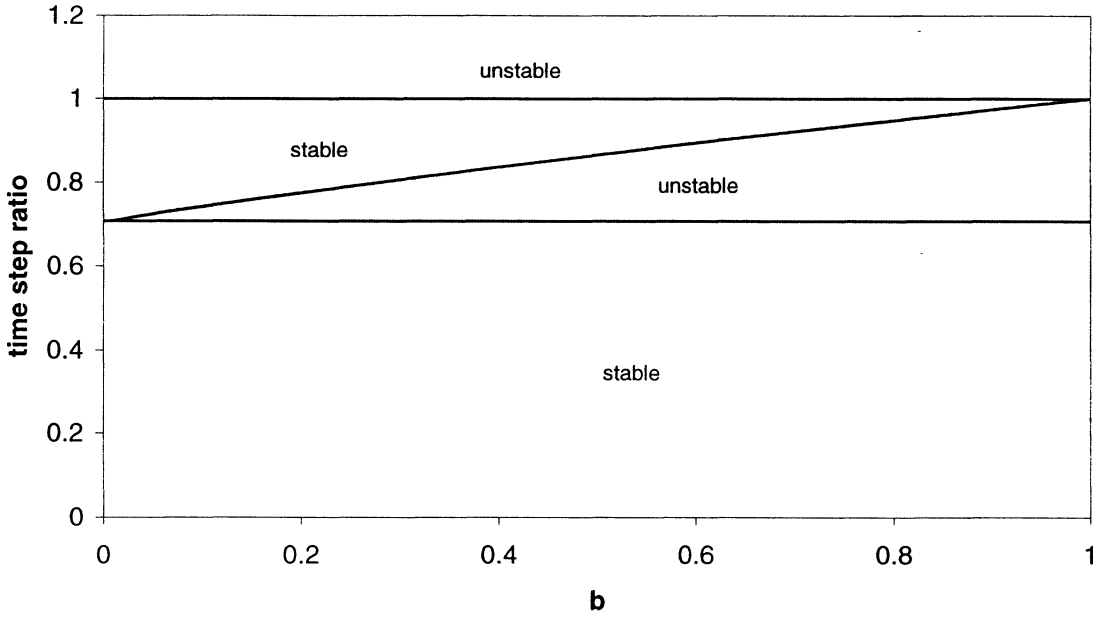

Figure 3.3 Stability map for one degree of freedom model

In the case of one degree of freedom model, the subcycled hourglass control approach introduces a new instability, which places an additional restriction on the stable time step for the central difference operator. We are interested in the stable region above the upper boundary because the proposed subcycling approach might not require a reduced time step. However, for higher degree of freedom systems, there will be a larger number of frequencies, and unstable regions may arise from the beating process between two close frequencies. We need to know the stability behavior of higher degree of freedom models. The greatest concern is whether there is a meaningful stable region above the upper boundary, which provides a way to avoid reducing the time step. This

problem is examined with the example of two, three, ten and one-hundred degree of freedom models.

3.4 Two degree of freedom model

Figure 3.4 shows the two degree of freedom mass-spring model. Here, we expect another unstable region to arise from the beating process. In order to find the second unstable region, we need to let the two natural frequencies of the model to be very close. If the two natural frequencies are far from each other, the second unstable region would fall into the area above $TSR = 1$, and it actually will not appear at all.

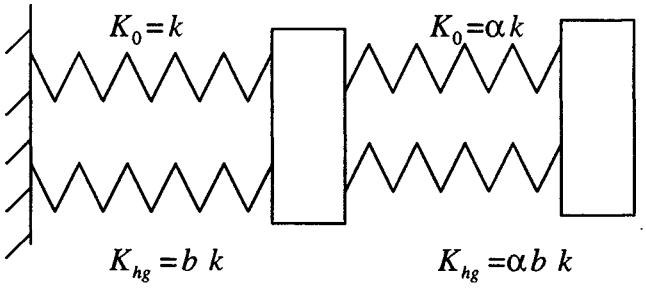

Figure 3.4 Two degree of freedom mass-spring model

We can obtain the stiffness and mass matrices of the model

$$K = k(1+b)\begin{bmatrix} 1+\alpha & -\alpha \\ -\alpha & \alpha \end{bmatrix},$$

$$M = k(1+b)\begin{bmatrix} 1+\alpha & 0 \\ 0 & \alpha \end{bmatrix} \qquad (3.4)$$

The mass distribution is determined intentionally to normalize the modes. The nature frequencies of the model are determined by solving the eigenvalue problem

$$\det[K - \lambda M] = 0,$$

where $\lambda = \omega^2$, so that

$$\omega = \sqrt{1 \pm \sqrt{\frac{\alpha}{\alpha+1}}} \qquad (3.5)$$

Here, we let $\alpha = 0.01$ to get two close frequencies: $\omega_1 = 1.049$, $\omega_2 = 0.949$. The critical time step is determined as $\Delta t_{cr} = 2/\omega_1$.

Figure 3.4 shows the stability map of the two degree of freedom model. There are two overlapped unstable regions corresponding to the critical time step for each mode. The lower boundary of lower unstable region lies around $TSR = 1/\sqrt{2}$. And the upper region corresponds to the lower region scaled by a factor ω_1 / ω_2.

Here, we see the reason why the two natural frequencies need to be close to each other. For example, if $\omega_1 / \omega_2 = 1.8$, theoretically the lower boundary of upper unstable region would lies around $TSR = 1.27$. We would not be able to detect the upper unstable

region on the stability map since it is all unstable above $TSR = 1$. Thus, only one unstable region would show up, and the stability map would not reflect the real characteristics of two degree of freedom models.

In the case of the two degree of freedom model, although there are two unstable regions, it is still not too troublesome to find the proper initial guess points TSR_1 and TSR_2.

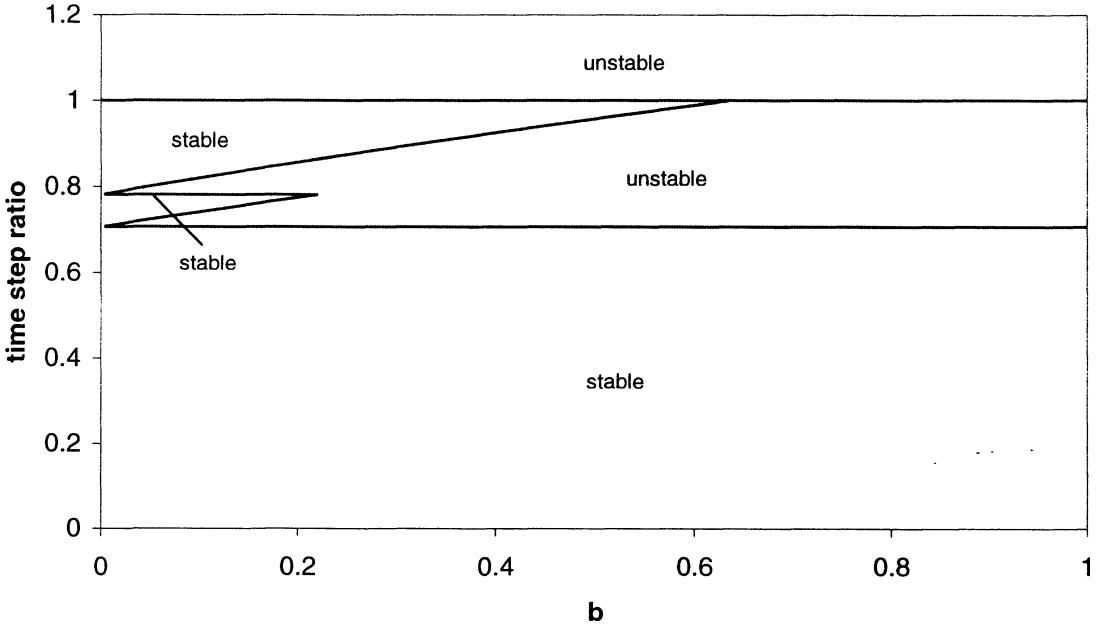

Figure 3.5 Stability map for two degree of freedom model

In Figure 3.5, the stability map confirms that another unstable region will arise from the beating process if the two natural frequencies are close enough. It can be

expected that for higher degree of freedom model, more unstable regions will arises from the beating process since there are more frequencies close to each other.

Notice that in Figure 3.5 there is still an attractive stable region between the unstable regions, although it is smaller than that in the case of one degree of freedom model. It may become even smaller as the degree of freedom gets higher and more unstable regions arise. This is examined in the next section with the use of three, ten and one hundred degree of freedom models.

3.5 Higher degree of freedom models

With the basic understanding of stability behavior of one and two degree of freedom models, we are ready to explore the stability of subcycled hourglass control approach applied to higher degree of freedom models. A generalized N degree of freedom model is established in Figure 3.6.

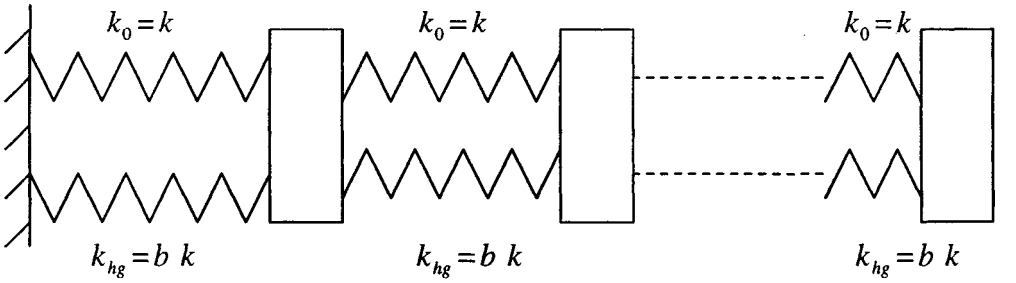

Figure 3.6 N degree of freedom model

The stiffness and mass matrices of the model are written in the form

$$K_n = \begin{bmatrix} 2 & -1 & & & & & & \\ -1 & 2 & -1 & & & & & \\ & -1 & 2 & -1 & & & & \\ & & \cdot & \cdot & \cdot & & & \\ & & & \cdot & \cdot & \cdot & & \\ & & & & \cdot & \cdot & \cdot & \\ & & & & & -1 & 2 & -1 \\ & & & & & & -1 & 1 \end{bmatrix} k(1+b)$$

$$M_n = \begin{bmatrix} 2 & & & & & & & \\ & 2 & & & & & & \\ & & 2 & & & & & \\ & & & \cdot & & & & \\ & & & & \cdot & & & \\ & & & & & \cdot & & \\ & & & & & & 2 & \\ & & & & & & & 1 \end{bmatrix} k(1+b) \qquad (3.6)$$

For the purpose of the study, the mass distribution is determined to be proportional to the stiffness matrix. The effect of doing so is to normalize the modes, so the maximum of the frequency is of the order of unity. Although this choice is arbitrary, it does not affect the generality of the model. The natural frequencies of the model can be determined by solving the eigenvalue problem, and the highest frequencies are used to calculate the critical time step $\Delta t_{cr} = 2/\omega_{\max}$.

Here we encounter a problem with the bisection method. As the degrees of freedom get higher, more unstable regions will arise because there will be more natural frequencies that are close to each other. It would be very difficult and expensive to find the proper initial guess points TSR_1 and TSR_2 when there are many unstable regions overlapped with each other between $TSR = 1/\sqrt{2}$ and $TSR = 1$. There can be several unstable regions between the initial guess points TSR_1 and TSR_2 (Figure 3.7).

Therefore, we applied the bisection method in the horizontal direction. For a certain TSR, we can easily choose two initial guess points, b_1 and b_2, and there will be only one unstable boundary between the two guess points.

The stability behavior of three, ten and one hundred degree of freedom models are shown in Figure 3.8, Figure 3.9, and Figure 3.10 respectively. As the system has more frequencies, more unstable regions arise from beating process between two close frequencies.

In Figure 3.8, there are only two unstable regions on the stability map for three degree of freedom model. This is because the highest frequency (1.366) is too far from the lowest frequency (0.366).

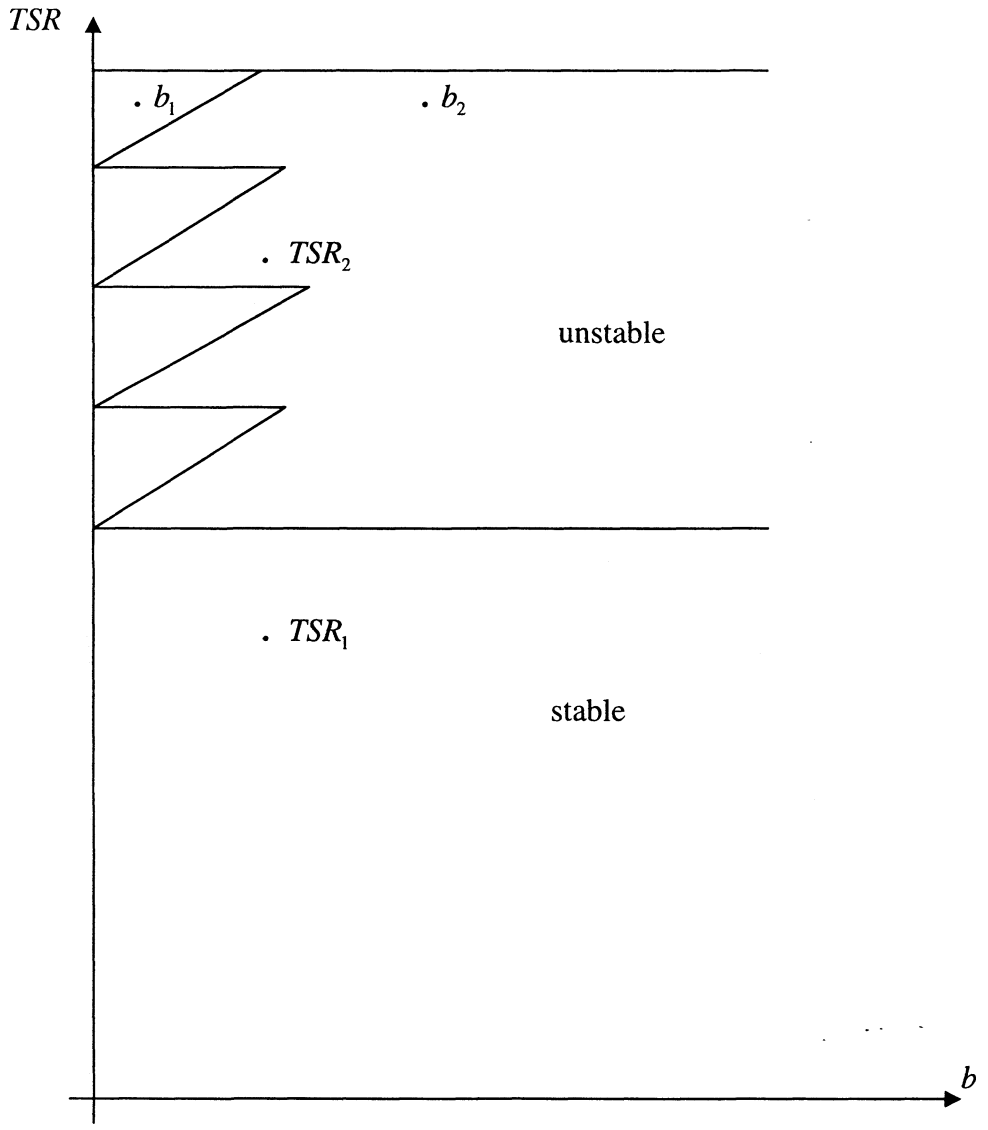

Figure 3.7 Use of bisection method in higher degree of freedom model

As shown in Figure 3.10, there are many overlapped unstable regions between $TSR = 1/\sqrt{2}$ and $TSR = 1$. For system with a large number of frequencies, it won't be worthwhile the effort to find the stable regions above the boundary $TSR = 1/\sqrt{2}$. Thus,

we may consider the new stability condition of the subcycled hourglass control approach is

$$\Delta t \le \frac{1}{\sqrt{2}} \Delta t_{cr} = \sqrt{2} / \omega_{\max} \qquad (3.7)$$

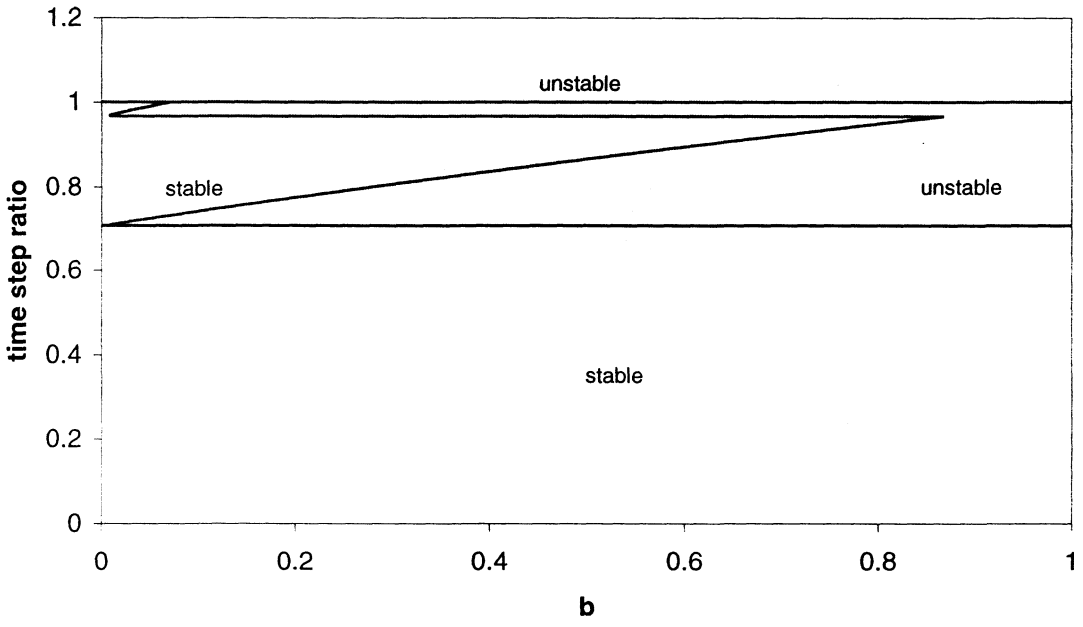

Figure 3.8 Stability map for three degree of freedom model

3.6 Discussion

The subcycling approach introduces a new instability, which imposes an unwelcome restriction on the time step. The reduced time step would negate the saving of subcycling the hourglass force. However, since the instability arises from beating process, it is expected that damping may restore stability. In next chapter, the effect of damping is explored.

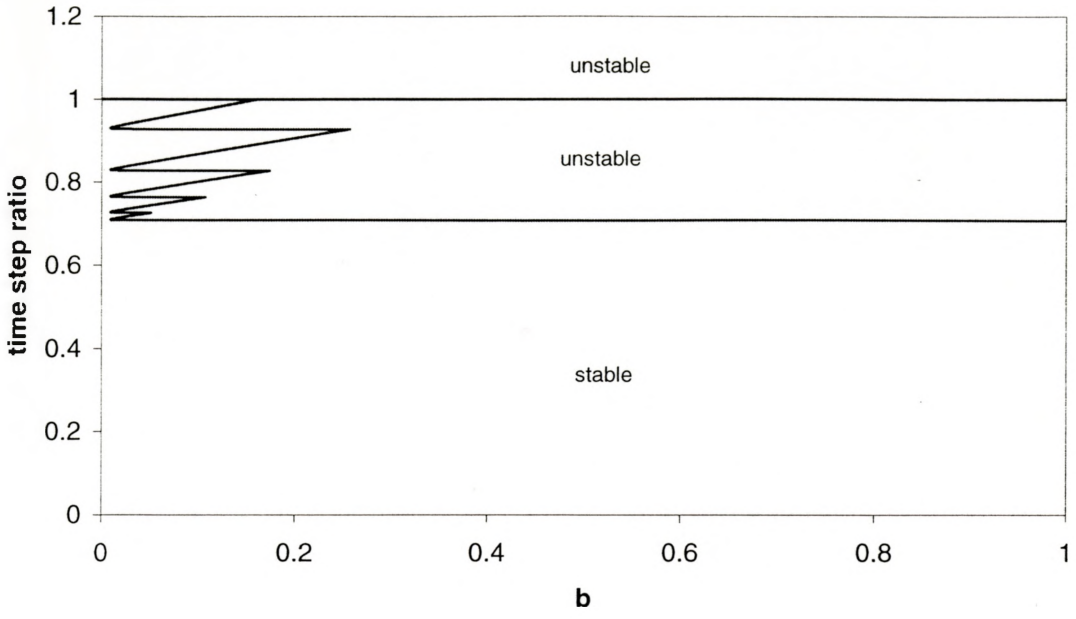

Figure 3.9 Stability map for ten degree of freedom model

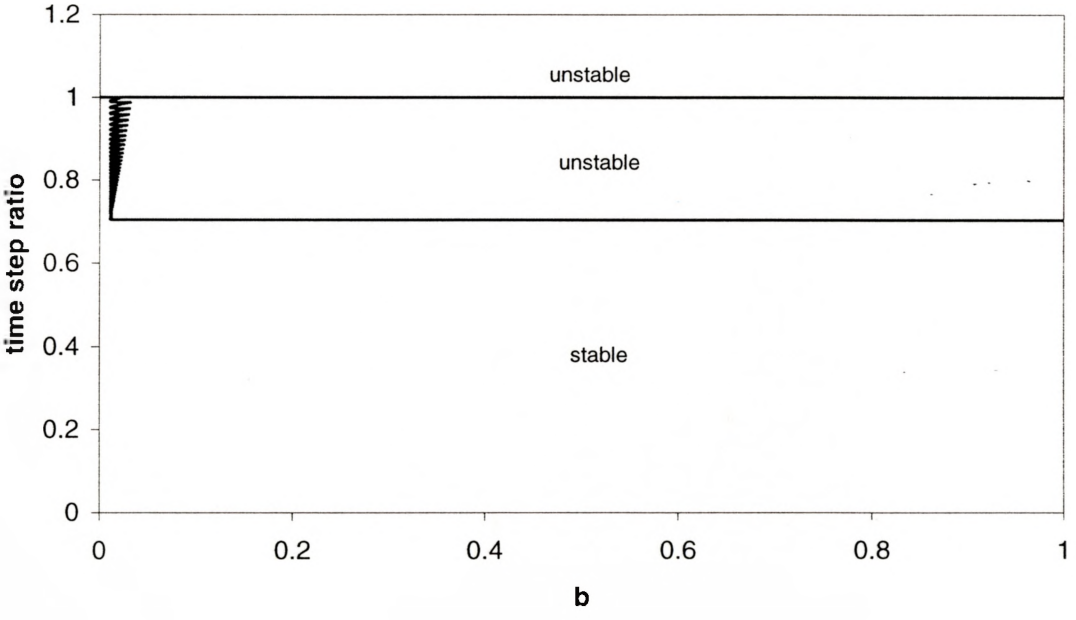

Figure 3.10 Stability map for one-hundred degree of freedom model

CHAPTER 4

DAMPING

As shown in Chapter 3, the proposed subcycled hourglass control approach requires reduced time step. This would make the proposed approach not so effective in terms of improving computational efficiency. However, since the instability arises from the beating process, we can expect that damping may restore the usual time step. In this chapter, the effect of damping on various multi-degree of freedom models is presented.

4.1 Introduction

In general, damping is the removal of energy from an oscillating system either by dissipation within the system or by transmission away from the system. Damping forces may have a controlling importance at the borderline between stable and unstable operation.

The equation governing the dynamic response of a finite element system can be written as

$$M\ddot{U} + C\dot{U} + KU = R \qquad (1.1)$$

Where M, K, and R are mass matrix, stiffness matrix and external force vector, and C is damping matrix.

The most popular approach to damping in direct integration is to let the damping matrix to be a linear combination of the mass and stiffness matrices

$$C = \alpha_1 M + \alpha_2 K \tag{4.1}$$

This is called proportional or Rayleigh damping.

Here, we set $\alpha_1 = 2\xi\omega$ and $\alpha_2 = 0$, therefore

$$C = 2\xi\omega * M \tag{4.2}$$

where ξ is called the damping ratio, and ω is the lowest frequencies. This is called mass proportional damping. The mass proportional damping matrix is diagonal for lumped mass matrix. Thus, computational efforts will be saved. In addition, mass proportional damping is efficient and well behaved.

4.2 Subcycling Algorithm with damping

The subcycling algorithm in Chapter 2 does not include any damping. Thus, a change in the subcycling algorithm needs to be made because here damping is involved. The acceleration and velocity of the system can be obtained by Equations (4.3)

$$\ddot{U}_n = \frac{1}{\Delta t}(\dot{U}_{n+1/2} - \dot{U}_{n-1/2})$$

$$\dot{U}_n = \frac{1}{2}(\dot{U}_{n+1/2} + \dot{U}_{n-1/2}) \tag{4.3}$$

Substituting $\ddot{U}_n$ and $\dot{U}_n$ into equation (1.2) yields

$$\frac{M}{\Delta t}(\dot{U}_{n+1/2} - \dot{U}_{n-1/2}) + \xi\omega M(\dot{U}_{n+1/2} + \dot{U}_{n-1/2}) = R - KU_n \tag{4.4}$$

Equation (4.4) can be written as

$$\dot{U}_{n+1/2}(1 + \xi\omega\Delta t) = \frac{\Delta t}{M}(R - KU_n) + \dot{U}_{n-1/2}(1 - \xi\omega\Delta t) \tag{4.5}$$

In our original algorithm, we calculated acceleration as

$$\ddot{U}_n = (R - KU_n)/M \tag{4.6}$$

Therefore, we calculate velocity as

$$\dot{U}_{n+1/2} = \frac{\Delta t \ddot{U}_n}{1 + \xi\omega\,\Delta t} + \frac{\dot{U}_{n-1/2}(1 - \xi\omega\,\Delta t)}{1 + \xi\omega\,\Delta t} \tag{4.7}$$

where ω is the frequency on which the damping ratio is based, and $\ddot{U}_n$ can be considered as the acceleration without damping. A revised algorithm for the subcycled hourglass control with damping is listed in Table 4.1.

With the new subcycling algorithm, the effect of damping is explored with the one degree of freedom model first. Then, the effect of damping to higher degree of freedom models is examined.

1. Initial conditions: $U_0, \dot{U}_{\frac{1}{2}}$

2. Determine force increment:

$$\overset{n-1/2}{F_0} = K_0 U_{n-1/2},$$

$$\overset{n-1/2}{F_{hg}} = K_{hg} U_{n-1/2}, \qquad \text{n is even}$$

$$\overset{n-1/2}{F_{hg}} = 0 \qquad , \qquad \text{n is odd}$$

3. Update force and calculate acceleration

$$F_{\text{int}}^{n} = F_{\text{int}}^{n-1} + \Delta t \overset{n-1/2}{F_0} + \Delta t \overset{n-1/2}{F_{hg}}$$

$$\ddot{U}_n = (F_{ext}^{n} - F_{\text{int}}^{n}) / M$$

4. Update velocity and displacement

$$\dot{U}_{n+1/2} = \frac{\Delta t \ddot{U}_n}{1+\xi\omega\,\Delta t} + \frac{\dot{U}_{n-1/2}(1-\xi\omega\,\Delta t)}{1+\xi\omega\,\Delta t}$$

$$U_{n+1} = U_n + \Delta t \dot{U}_{n-1/2}$$

5. Repeat steps 2-4 to the end of analysis

Table 4.1 Subcycling algorithm with damping

4.3 One degree of freedom model with damping

First, a small damping ratio ($\xi = 0.1$) is chosen to reveal the effect of damping. Figure 4.1 shows that the unstable region of the system with damping is much smaller than that of the system without damping. Thus, damping is very effective in restoring the stability of the subcycled hourglass control approach. We expect that the unstable region will become smaller as we increase the damping ratio ξ.

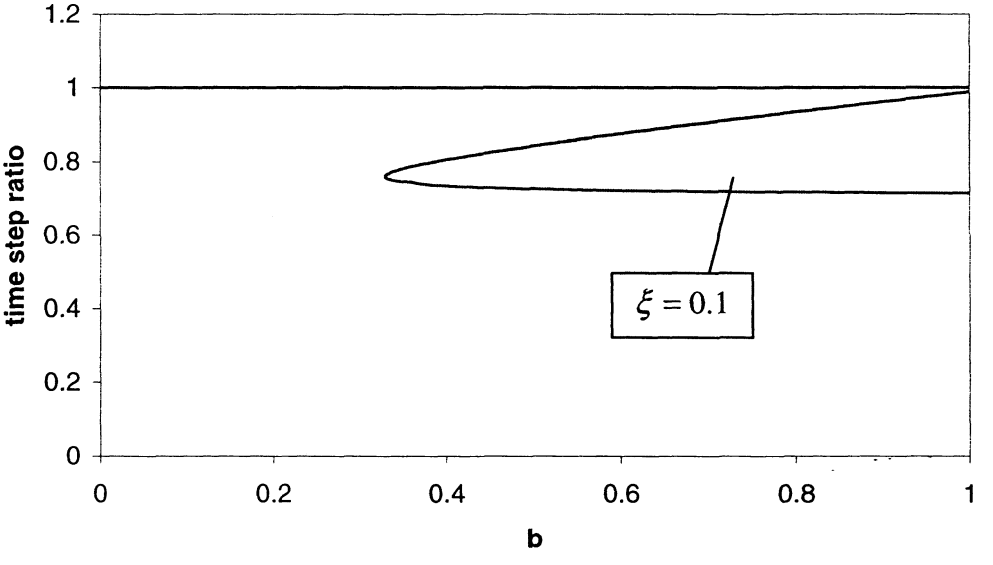

Figure 4.1 Stability map for one degree of freedom with damping ratio 0.1

Figure 4.2 shows the stability maps for different damping ratios ($\xi = 0.1$, 0.2, 0.25). It is found that as the damping ratio becomes larger, the unstable region becomes smaller. In effect, when $\xi \geq 0.29$, no instability is encountered as long as time step ratio is less than 1. Thus, adding damping is an effective way to restore stability.

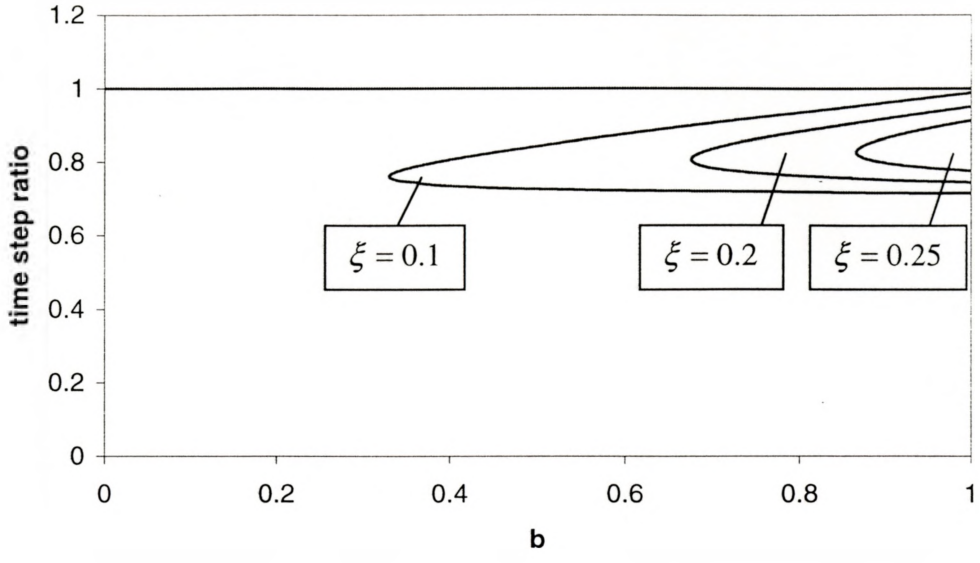

Figure 4.2 Stability maps for one degree of freedom model with $\xi = 0.1, 0.2, 0.25$

4.4 Higher degree of freedom models with damping

The effect of damping on higher degree of freedom models is shown in Figure 4.3 to Figure 4.6. In the figures, the stability maps of the models with damping are compared to the models without damping ($\xi = 0$).

For higher degree of freedom models, the lowest frequencies are small. For example, the lowest frequency of ten degree of freedom model is 0.111. Therefore, for the same damping ratio ($\xi = 0.1$) on the lowest ω, the effect of damping is not as significant as that in one degree of freedom model. This is evident when we compare Figure 4.5 with Figure 4.1. And we notice that in the two degree of freedom model, the

effect of damping is still significant, while in the three degree of freedom model, the effect is much less significant. In the cases of 100 degree of freedom model, the lowest frequency (0.01) is so small that the damping ratio is chosen to be 0.5 in order to reveal the effect of damping.

Another feature in the stability maps is that for lower frequencies, the effect of damping is more significant. For example, in Figure 4.3, with damping ratio $\xi = 0.1$, the upper unstable region is clearly smaller than lower unstable region. This is the characteristic of mass proportional damping.

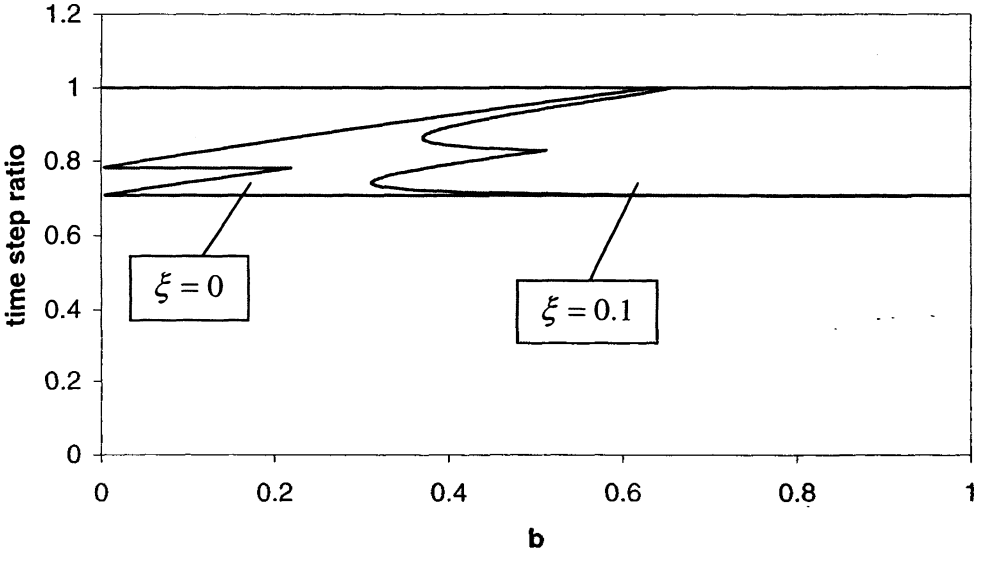

Figure 4.3 Stability maps for two degree of freedom model with $\xi = 0, 0.1$.

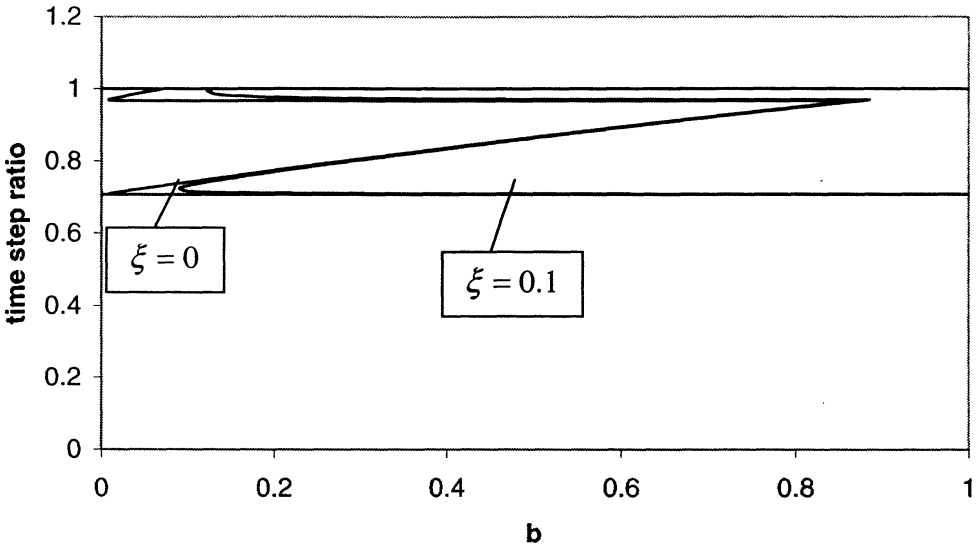

Figure 4.4 Stability map for three degree of freedom model with $\xi = 0, 0.1$

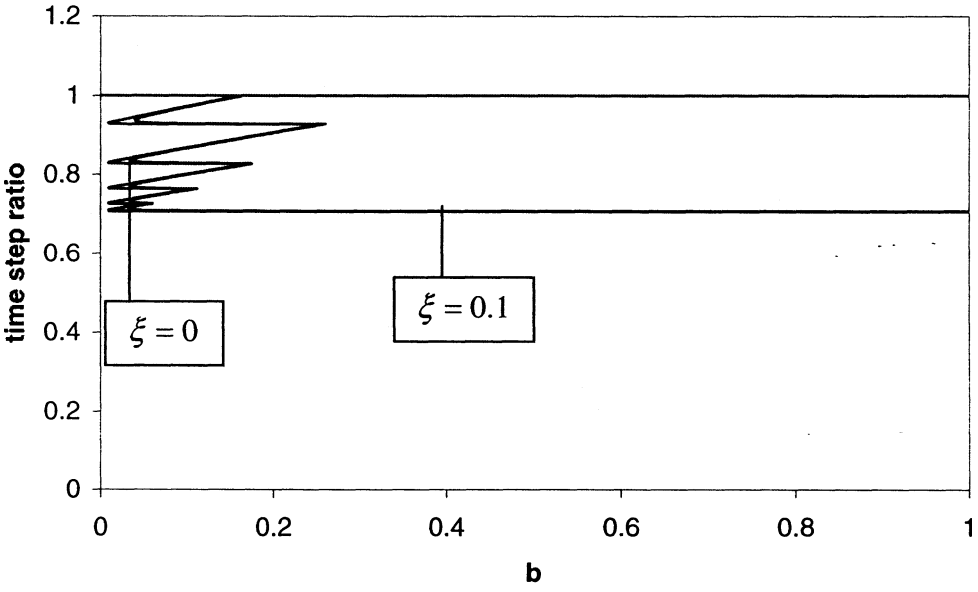

Figure 4.5 Stability map for ten degree of freedom model with $\xi = 0, 0.1$

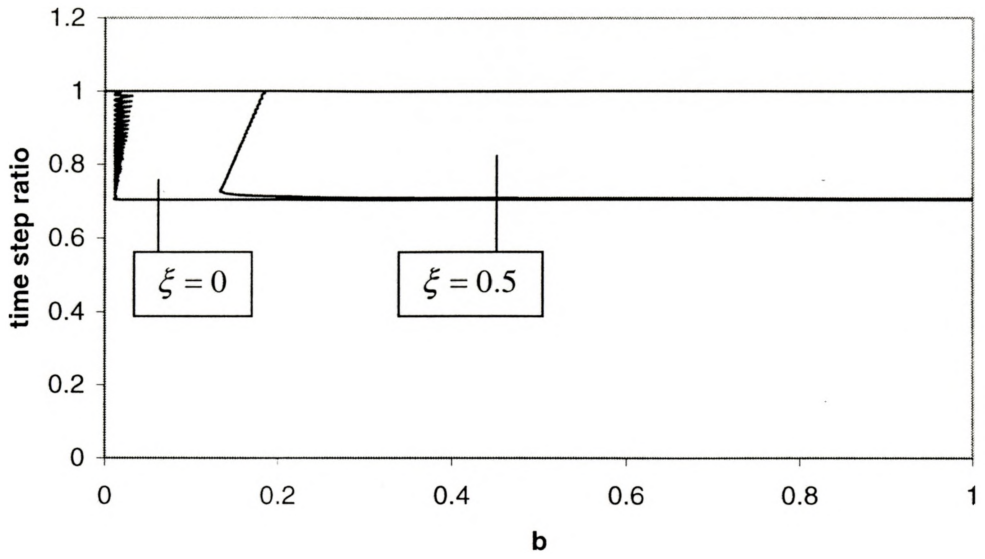

Figure 4.6 Stability map for one hundred degree of freedom models with $\xi = 0, 0.5$

Figure 4.7 shows the effect of increasing the damping ratio in ten degree of freedom model. The figure indicates that damping could effectively restore the usual stable time step for complex problems with many degrees of freedom.

4.5 Dynamic Relaxation

In the preceding sections, we explored the effect of damping in transient problems. In those cases, the damping matrices are predetermined and retained for the analysis. Another commonly used method in finite element analysis is dynamic relaxation, or DR, which employs different damping ratio to the different modes of the response.

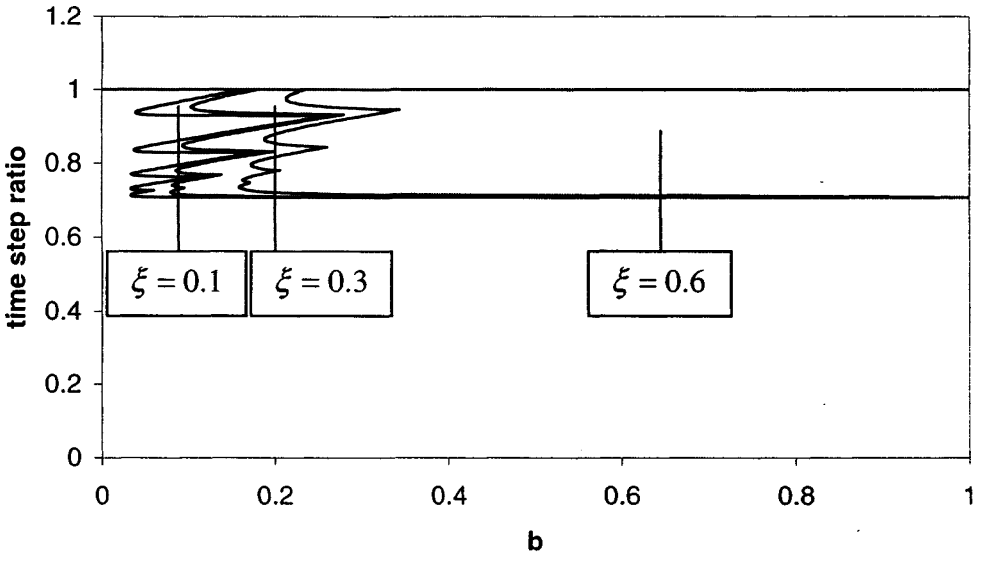

Figure 4.7 Stability map for ten degree of freedom models with ξ=0.1, 0.3, 0.6

Since 1965, numerous papers (Day [19], Otter [20], Brew and Brotton [21], Pica and Hinton [22], Papadrakakis [23], and Underwood [24]) have been produced that describe the use of dynamic relaxation in the solution of finite difference approximations to the partial differential equations. In the paper by Oakley and Knight [25], an overview of previous works is presented.

For the mass-spring model, the effect of damping in dynamic relaxation problems is explored below.

In dynamic relaxation problems, the damping matrix C, is given by

$$C = 2\xi\omega * M$$

where ω is the undamped natural frequency corresponding to the mode that most closely resembles the current response. An approximation for ω can be obtained as

$$\omega \approx \sqrt{\frac{\dot{U}^T (F_{\text{int}}^n - F_{\text{int}}^{n-1})/\Delta t}{\dot{U}^T M \dot{U}}} \qquad (4.8)$$

where $\dot{U}$ is the current velocity vector, and superscript T indicates transpose of the matrix. Equation 4.8 is itself an approximation to the Rayleigh quotient 4.9

$$\omega \approx \sqrt{\frac{U^T K U}{U^T M U}} \qquad (4.9)$$

where U is the current displacement vector, K is the current tangent stiffness matrix [26].

Note that the frequency needs to be updated before the velocity is updated, otherwise we will be using next step's velocity to calculate the frequency instead of the current step's velocity. For the first step of calculation, since the current velocity vector is not yet available to obtain ω, the highest frequency will be used in the velocity update equation.

$$\dot{U}_{n+1/2} = \frac{\Delta t \ddot{U}_n}{1+\xi\omega\,\Delta t} + \frac{\dot{U}_{n-1/2}(1-\xi\omega\,\Delta t)}{1+\xi\omega\,\Delta t} \qquad (4.7)$$

The algorithm for dynamic relaxation problems is listed in Table 4.2

1. Initial conditions: $U_0, \dot{U}_{-\frac{1}{2}}$

2. Determine force increment:

$$\dot{F}_0^{n-1/2} = K_0 \dot{U}_{n-1/2},$$

$$\dot{F}_{hg}^{n-1/2} = K_{hg} \dot{U}_{n-1/2}, \qquad \text{n is even}$$

$$\dot{F}_{hg}^{n-1/2} = 0 \qquad , \qquad \text{n is odd}$$

3. Update force and calculate acceleration

$$F_{\text{int}}^n = F_{\text{int}}^{n-1} + \Delta t \dot{F}_0^{n-1/2} + \Delta t \dot{F}_{hg}^{n-1/2}$$

$$\ddot{U}_n = (F_{ext}^n - F_{\text{int}}^n)/M$$

4. Update frequency, velocity, and displacement

$$\omega \approx \sqrt{\frac{\dot{U}^T (F_{\text{int}}^n - F_{\text{int}}^{n-1})/\Delta t}{\dot{U}^T M \dot{U}}}$$

$$\dot{U}_{n+1/2} = \frac{\Delta t \ddot{U}_n}{1+\xi\omega\,\Delta t} + \frac{\dot{U}_{n-1/2}(1-\xi\omega\,\Delta t)}{1+\xi\omega\,\Delta t}$$

$$U_{n+1} = U_n + \Delta t \dot{U}_{n-1/2}$$

5. Repeat steps 2-4 to the end of analysis

Table 4.2 Subcycling algorithm in dynamic relaxation

In addition, when ω cannot be obtained due to dividing by zero or square root of a negative number in the Rayleigh quotient, the highest frequency will be used instead.

Figure 4.8 shows the stability map of the ten degree of freedom model in dynamic relaxation problems with ξ=0.1. The unstable regions are much smaller than those in Figure 4.5, which shows the stability map of ten degree of freedom model in transient problems. The effect of damping in dynamic relaxation problems is much more significant than in transient problems.

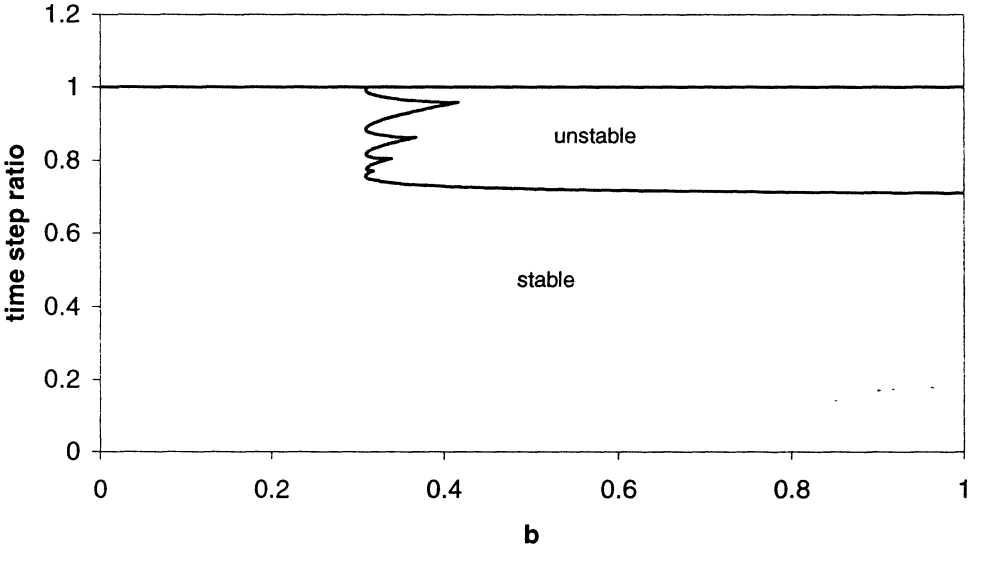

Figure 4.8 Stability map for ten degree of freedom model in DR with ξ=0.1

With Figure 4.9, which is obtained by putting stability maps in DR and in transient problems together, we can compare the damping effect on the ten degree of freedom model in DR (Figure 4.8) with that in transient problems (Figure 4.5). The

unstable regions on the left of Figure 4.9 are the stability map for the ten degree of freedom model in transient problems with ξ=0.1 on the lowest frequency, and the smaller unstable region in Figure 4.9 is the stability map for the ten degree of freedom model in dynamic relaxation. It is evident that damping in DR is more effective than in transient problems to restore the stability of the subcycled hourglass control approach. This is because the damping matrix C in dynamic relaxation is determined to ensure that any mode is critically damped. If any mode starts to grow, the adaptive damping will increase accordingly.

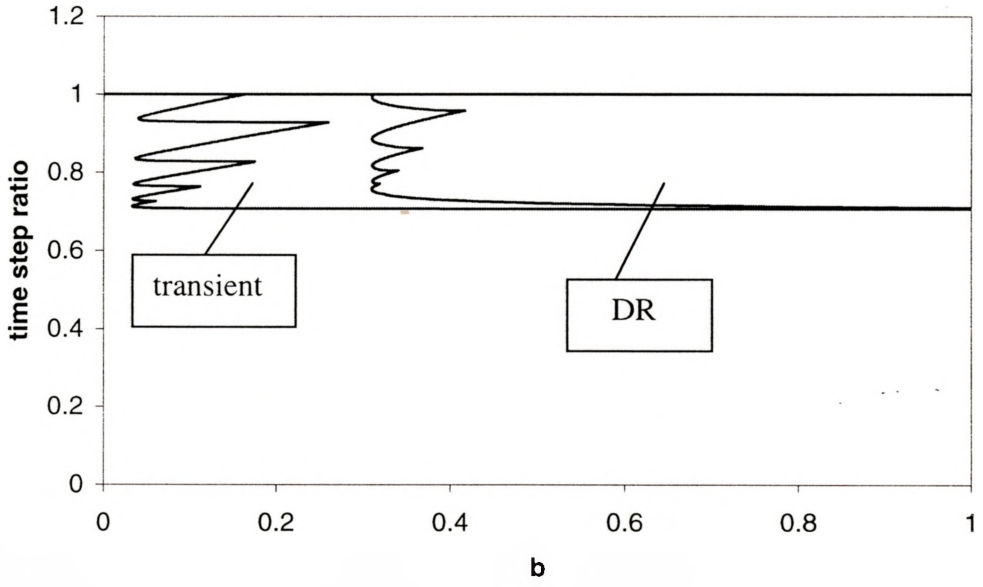

Figure 4.9 Stability map comparison between transient and DR for ten degree of freedom model with ξ=0.1

Figure 4.10 shows how the unstable regions are getting smaller as we increase the damping ratio ξ in DR. We find that when the damping ratio ξ is chosen to be 0.2, the unstable regions are rather small. In fact, when the damping ratio ξ is larger than 0.28, no instability is encountered.

Figure 4.11 shows the stability maps for one hundred degree of freedom model in DR with different damping ratio ξ (ξ=0.1, 0.15, 0.2). As the damping ratio ξ increases, the unstable regions shrink rapidly. When the damping ratio ξ is larger than 0.28, no instability appears. Thus, in dynamic relaxation problems, damping can very effectively restore stability of the subcycled hourglass control approach.

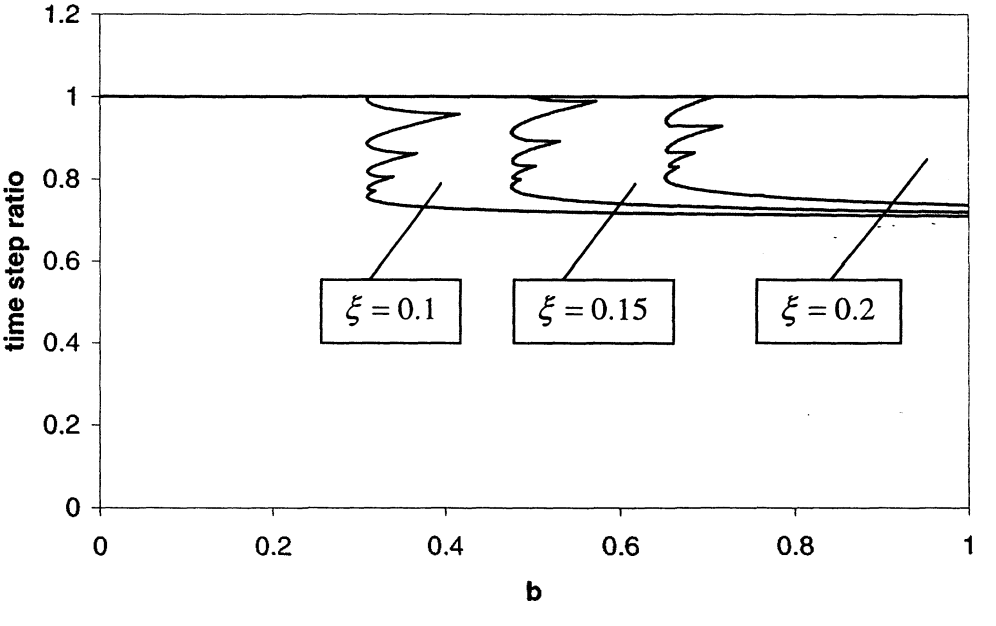

Figure 4.10 Stability maps for ten degree of freedom model in DR

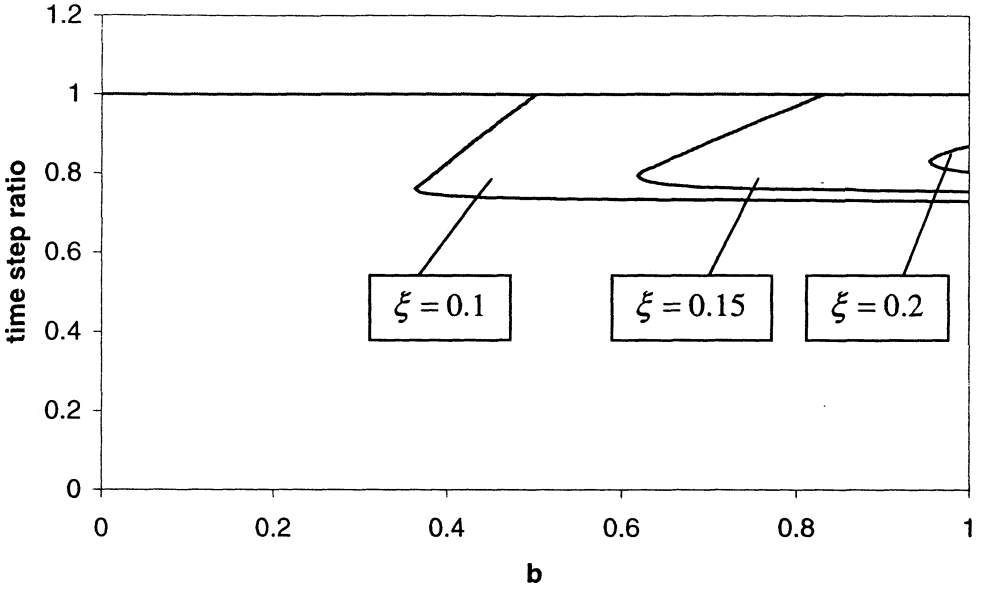

Figure 4.11 Stability maps for one hundred degree of freedom model in DR

4.6 Discussion

For transient problems, damping must be limited so as not to distort the true response of the system. This can be a disadvantage unless stiffness proportional damping alone can maintain stability. However, for static and quasi-static problems, where damping and mass may be selected arbitrarily, sufficient damping can be ensured to restore the usual time step. Therefore, in many transient problems, the subcycling approach can be applied to significantly improve the computational efficiency.

The dynamic relaxation method employs mass proportional damping and will apply different damping ratios to the different modes of response. In the one degree of

freedom model, it provides a critically damped system, and no instability appeared as long as the secondary stiffness is less than the primary stiffness. In higher degree of freedom models, the adaptive damping will increase if any modes begin to grow. Thus, no unstable behavior appeared either.

In practical finite element analysis, damping is involved in large class of problems. For example, a wide variety of non-inertial transient and quasi-static problems can be tackled with explicit methods using artificial damping. Metal forming, stamping and cutting operations are good candidates for some artificial damping [16]. It can be expected that in many cases, such as dynamic relaxation problems, the damping is sufficient to restore the stability. Therefore, the subcycled hourglass control approach can be applied widely to the finite element analysis without requiring a reduced time step. This is highly advantageous in improving computational efficiencies of the analysis for complex problems with a large number of elements.

CHAPTER 5

Accuracy

Aside from stability, accuracy is an important issue that we need to consider, and it is explored in this chapter. Since the one point quadrature and hourglass control approach already involves considerable approximation, the importance of accuracy is reduced. As long as spurious motion is controlled, the actual hourglass forces are of little interest. Still, the overall accuracy needs to be examined. In this chapter, transient and dynamic relaxation problems will be used to compare the overall accuracy of the proposed subcycling approach to that of normal integration.

5. 1 Transient Problems

For transient problems, significant truncation error occurs in the time integration of the modes of the highest frequencies, which are almost never accurately represented. In modes of frequencies that are lower than the subcycled frequency, appropriate accuracy is more easily found. Since frequencies required for stability are lower than that required for accuracy of the time integration, overall accuracy can be achieved.

This can be illustrated by comparing the results of the proposed approach and usual approach. First, we use one degree of freedom model with no damping. Time step

ratio, TSR, is set to be 0.9, and b is set to be 0.15. TSR and b are chosen to make the subcycled approach stable. For a step load applied at the initial time, Figure 5.1 shows the result of normal central difference operator with no subcycling, and Figure 5.2 shows the result of subcycled approach. It appears that the overall equilibrium point about which oscillation occurs is not adversely affected.

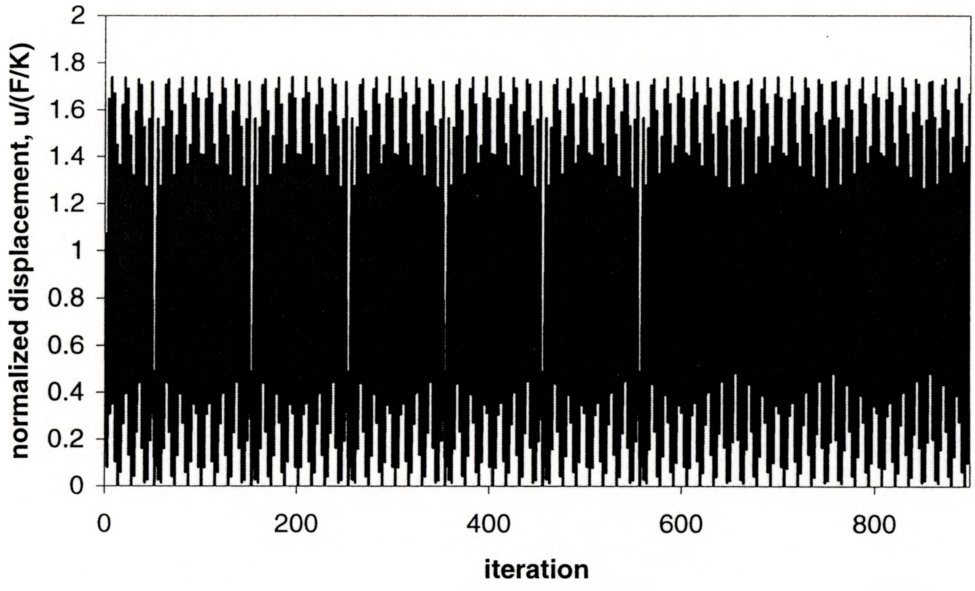

Figure 5.1 One degree of freedom model displacement with usual central difference operator (TSR=0.9, b=0.15 and ξ=0.0)

Next, consider the one degree of freedom model with damping ratio $\xi = 0.1$. Figure 5.3 and Figure 5.4 show the results of usual central difference operator and the subcycled approach respectively. Comparing the figures, we find that when damping is involved, not only stability can be somewhat restored, but also accuracy can be improved.

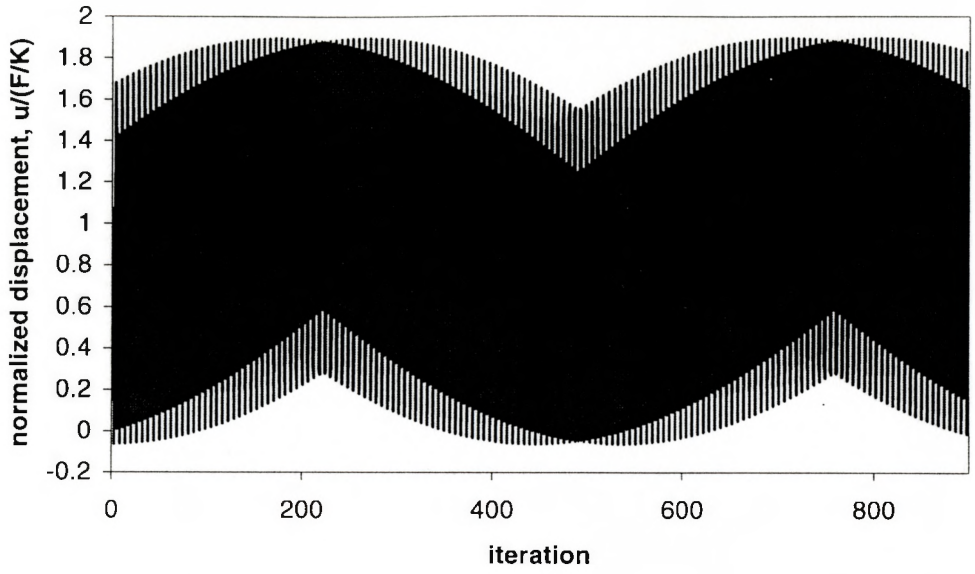

Figure 5.2 One degree of freedom model displacement with the subcycling approach (TSR=0.9, b=0.15 and ξ=0.0)

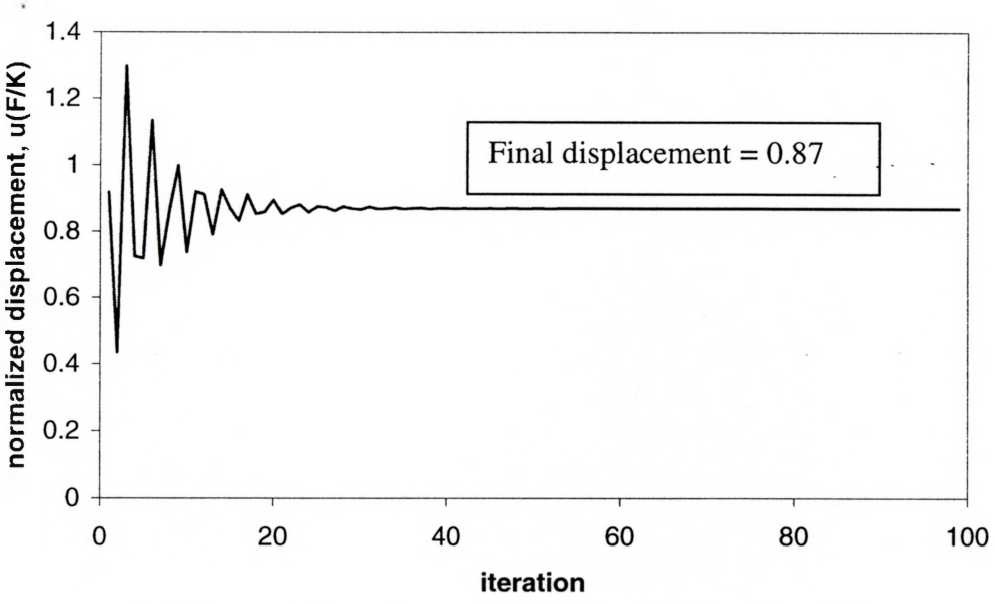

Figure 5.3 One degree of freedom model displacement with usual central difference operator (TSR=0.9, b=0.15 and ξ=0.1)

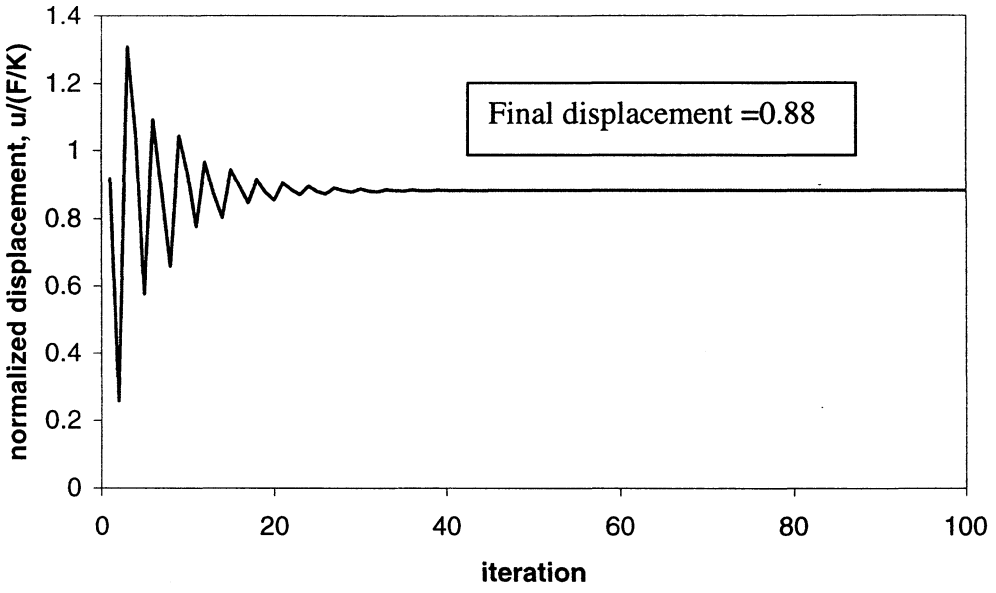

Figure 5.4 One degree of freedom model displacement with the subcycling approach (TSR=0.9, b=0.15 and ξ=0.1)

5.2 Dynamic Relaxation Problems

For dynamic relaxation problems, the study of mass-spring model demonstrates that accuracy is affected by the hourglass subcycling and accuracy can also be affected by damping ratio ξ, time step ratio TSR and b. Satisfactory accuracy can be achieved with a favorable set of parameters. However, in actual finite element analysis, the hourglass stiffness is not entirely parallel to the primary stiffness. Therefore, much better accuracy is obtained in finite element analysis.

First, we use an example of ten degree of freedom model to examine the overall accuracy of the subcycling approach. In the example, *TSR* is 0.9, b is 0.15, and ξ is 0.1.

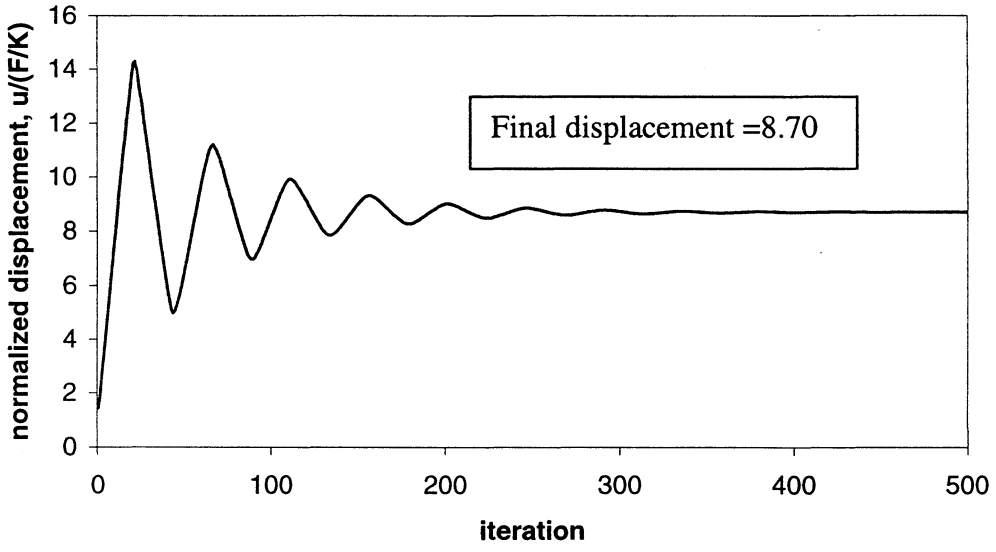

Figure 5.5 One degree of freedom model displacement with usual central difference operator in DR (*TSR*=0.9, b=0.15 and ξ=0.1)

Comparing Figure 5.5 and Figure 5.6, we find that in dynamic relaxation the overall accuracy of the subcycled approach is not as satisfactory as that in transient problems. It represents a 6.78% error. This is mainly because the damping ratio is so small that the critical damping is not achieved. When we let damping ratio ξ to be 1, the accuracy of the subcycling approach is improved.

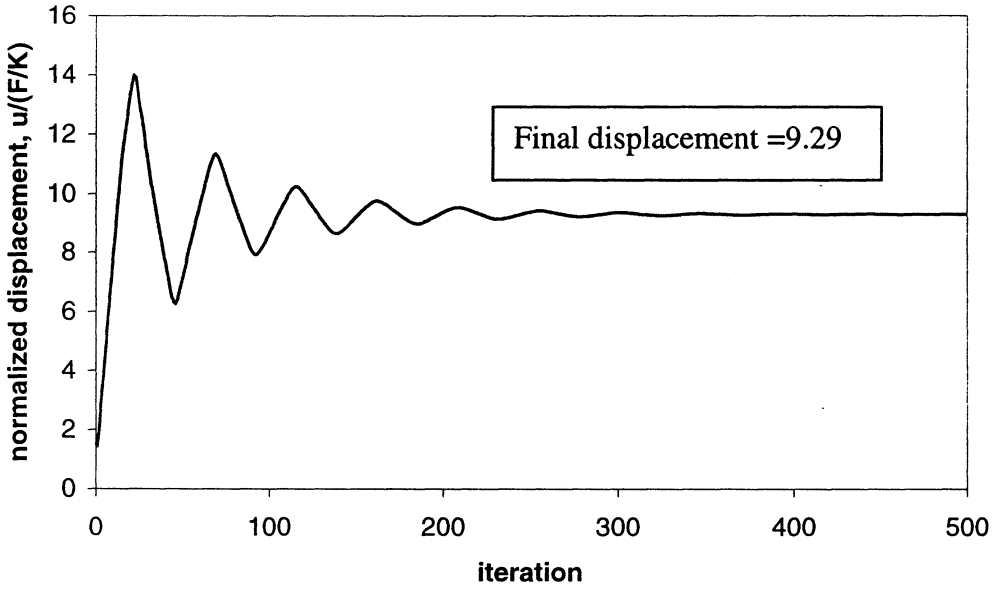

Figure 5.6 One degree of freedom model displacement with the subcycling approach in DR (TSR=0.9, b=0.15 and ξ=0.1)

Accordingly, in the ten degree of freedom model, we let TSR to be 0.9, ξ to be 1, and keep b to be 0.15. Figure 5.7 and Figure 5.8 show the results of the usual central difference operator and the subcycled approach with the new setting respectively. The result of the usual central difference operator remains the same (8.70), while the result of the subcycled approach declines to 9.01. Thus, the error declines to 3.56%. It demonstrates that in dynamic relaxation problems, better accuracy can be achieve with higher damping ratio ξ in the subcycled approach.

In addition, increasing *TSR* also gives us better accuracy. For example, with $\xi=1$ and $b=0.15$, the result with the subcycled approach is 9.09 when *TSR* is 0.5, it declines to 9.07 when *TSR* is 0.7, and the result becomes 9.01 when *TSR* is 0.9 (see Table 5.1).

Naturally, we consider choosing *TSR* to be 0.99 to achieve the best accuracy. However, when *TSR* is close to 1, the time step is close to the stability limit. Consequently, the numerical solution will display spurious beating in which the amplitude of response repeatedly grows and decays [1]. Therefore, we choose *TSR* to be 0.9 instead of 0.99.

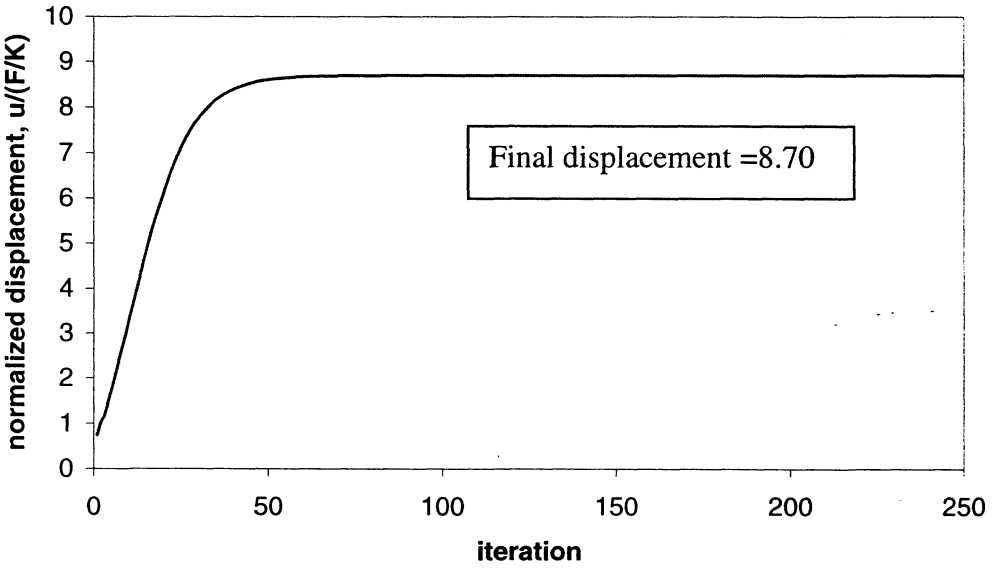

Figure 5.7 One degree of freedom model displacement with the usual central difference operator in DR (*TSR*=0.9, *b*=0.15 and $\xi=1$)

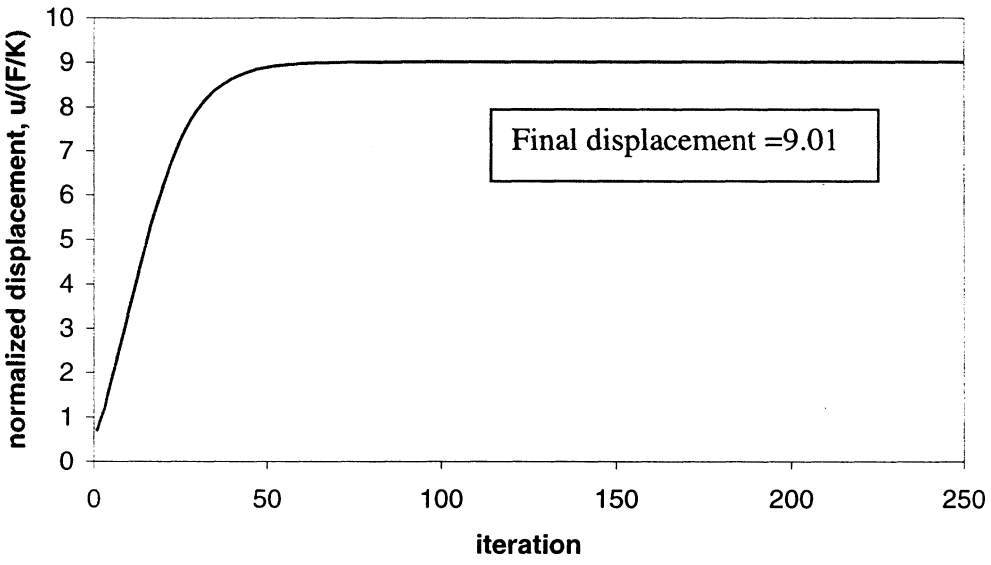

Figure 5.8 One degree of freedom model displacement with the subcycled approach in DR (*TSR*=0.9, *b*=0.15 and ξ=1)

TSR	0.5	0.7	0.9
Result	9.09	9.07	9.01
Error	4.48%	4.25%	3.56%

Table 5.1 Accuracy with different *TSR*

Apparently, a lower *b* can also give us better accuracy, because the hourglass forces will be less significant in the calculation. In the previous cases, *b* is set to be 0.15. The displacement solution with the subcycled approach is 9.01, while the solution with the usual central difference operator is 8.70. That represents an error of 3.56%. Here we

change b to be 0.05, and keep other parameters unchanged. Figure 5.9 and Figure 5.10 shows the displacement results for the usual central difference operator and the subcycled approach respectively. The error is trimmed to 1.68%, with the result of subcycled approach to be 9.68 and the result of the usual approach to be 9.52.

Thus, for the mass-spring model in dynamic relaxation problems, by choosing a lower b and a higher damping ratio, satisfactory accuracy can be achieved. Use of a higher time step ratio can also improve accuracy, but it should not be close to 1. If time step ratio is close to 1, the solution will exhibit beating. For finite element models, better accuracy is found because the hourglass forces in finite element models mainly are orthogonal to the one-point quadrature forces.

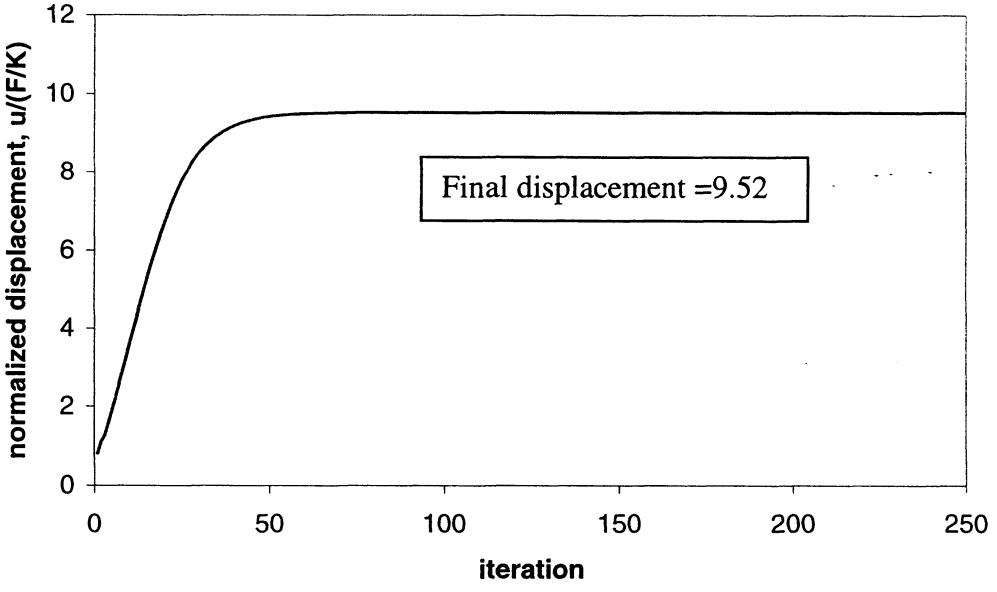

Figure 5.9 One degree of freedom model displacement with the usual central difference (TSR=0.9, b=0.05 and ξ=1)

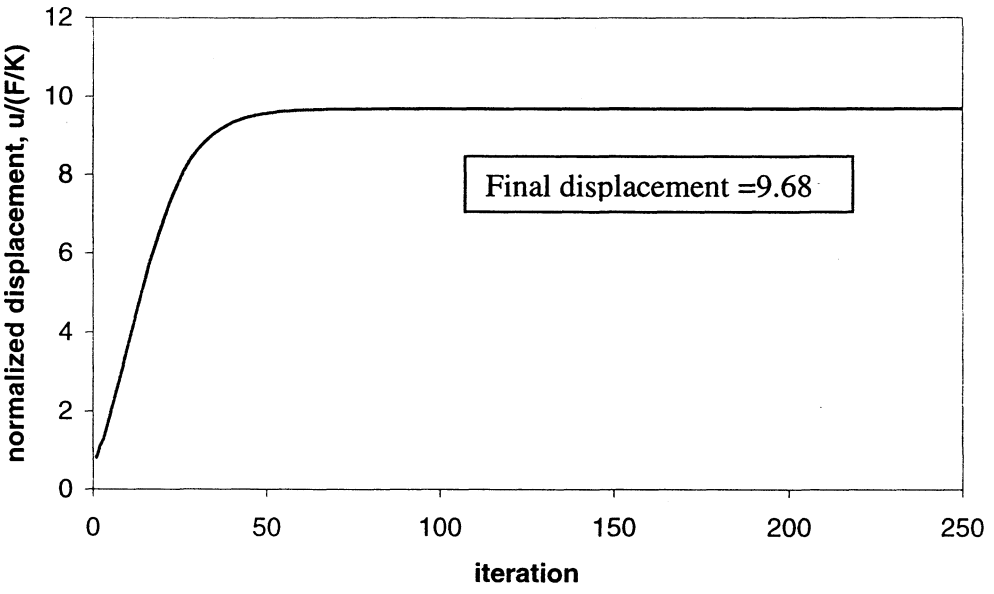

Figure 5.10 One degree of freedom model displacement with the subcycling approach (TSR=0.9, b=0.05 and ξ=1)

5.3 Discussion

The subcycling method will not significantly affect the accuracy of the solution as long as the stability is ensured. So far, all the studies are based on the simplified mass-spring models. It is essential to implement the proposed approach into an explicit finite element program. This is demonstrated on a three-dimensional example in next chapter.

CHAPTER 6

Finite Element Test Case

In this chapter, a finite element model is used to demonstrate the subcycling in a finite element context. Transient and dynamic relaxation problems will be examined. In each problem, stability and accuracy behavior are explored.

6.1 Finite element implementation

To prove applicability to more complex models, the subcycling algorithm of Table 2.1 has been implemented into an explicit finite element code. The code, H3DMAP, Sauve [30], has been modified to allow for transient and dynamic relaxation. The primary stiffness is determined by one point quadrature, and the secondary stiffness is determined by the hourglass stiffness. The exact determination of the hourglass stiffness is given by

$$K_{hg} = \Gamma C_h \Gamma^T \qquad (6.1)$$

where Γ is a matrix of hourglass basis vectors and C_h is the hourglass constitutive matrix. More details of the Γ and C_h terms are given in [11].

However, instead of forming stiffness directly, internal forces are equivalently determined on an element by element basis. The hourglass force increments are evaluated every other step, and are stored for the steps where evaluation is skipped [16].

6.2 Transient response

A finite element model is established representing a simply supported beam with a central transverse load. Figure 6.1 shows the 3-D mesh, and Figure 6.2 shows the transient deformed shape without hourglass subcycling. Note that the deformed shape is shown in a magnified way to make the small deformation visible. The system oscillates about the equilibrium position corresponding to the static load, as shown in Figure 6.3, and the displacement has been normalized with respect to the static displacement of the finite element model.

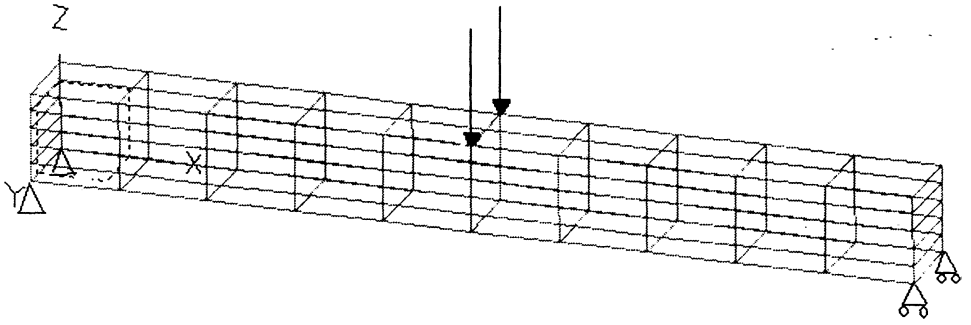

Figure 6.1 Mesh for beam model

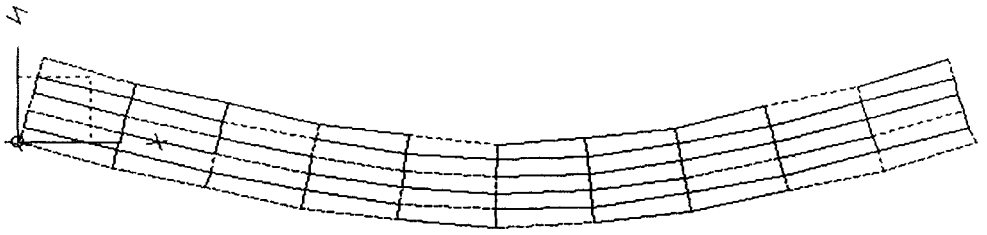

Figure 6.2 Transient deformation without hourglass subcycling

When the subcycling scheme is used, the transient response starts with the expected course, but an oscillation at higher frequency accompanies the main response and grows into an instability eventually as shown in Figure 6.4.

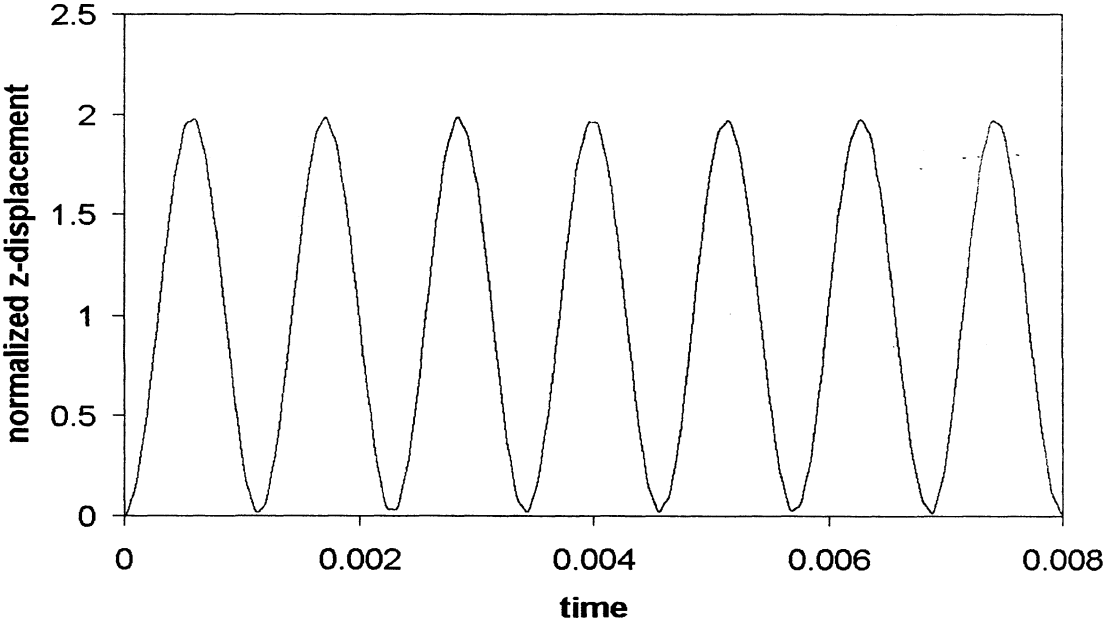

Figure 6.3 Transverse deflection of beam without hourglass subcycling

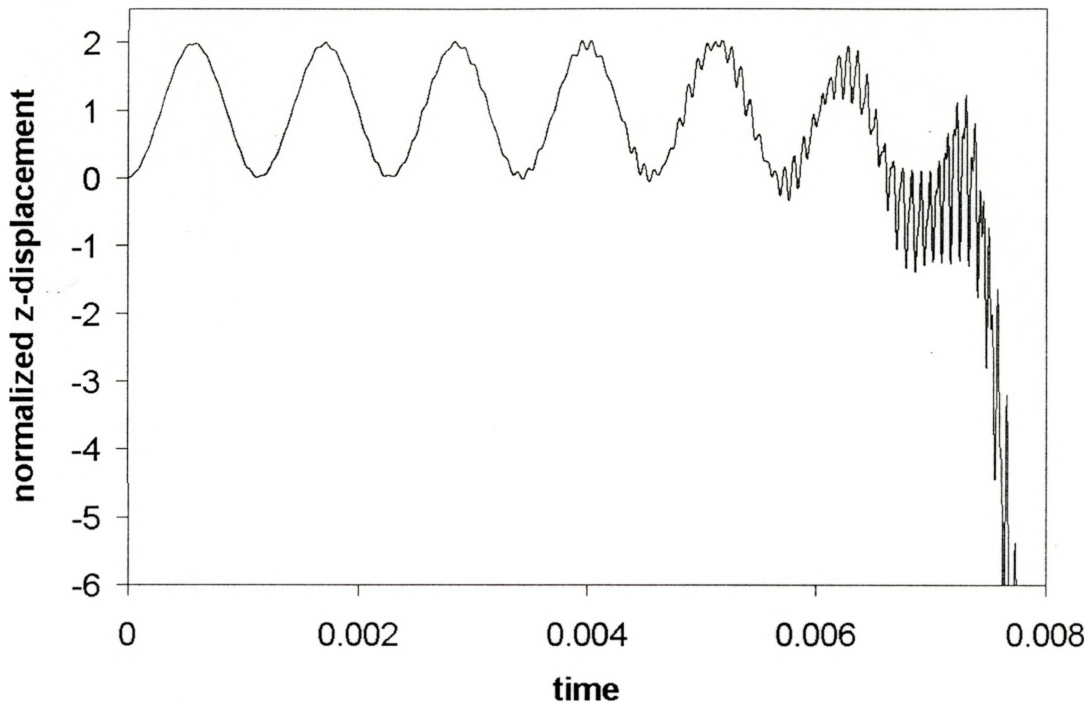

Figure 6.4 Transverse deflection of beam with subcycling

In the above case, the time step is set to be slightly above the $1/\sqrt{2}$ factor required for absolute stability, and no damping is used. The penalty factor applied to the hourglass control is 0.01 of full quadrature so that this case is in the region to the extreme left of the stability map in Figure 3.2. We terminate the problem after it runs for about 10000 time steps. Figure 6.5 shows the deformed geometry prior to program termination, and the unstable deformations appear to be mainly hourglass modes. The result demonstrates that the finite element model has the same stability characteristics as the more understandable mass-spring models.

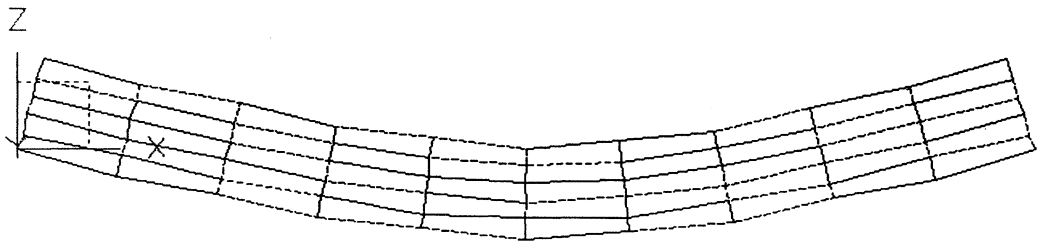

Figure 6.5 Transient deformation with hourglass subcycling

Note that in the above case no damping is applied. In Chapter 4, we find that damping can restore stability of the subcycled hourglass approach. Therefore, we add damping onto the above finite element model expecting stability to be restored. With damping applied to the model, the transverse deflection of beam without and with subcycling is shown in Figure 6.6 and Figure 6.7 respectively. It demonstrates that damping can effectively restore stability of the subcycled hourglass approach. In addition, satisfactory accuracy is achieved with the subcycling approach when damping is applied.

The transient deformed shapes for the normal approach and the subcycling approach when damping is applied are shown in Figure 6.8 and Figure 6.9 respectively.

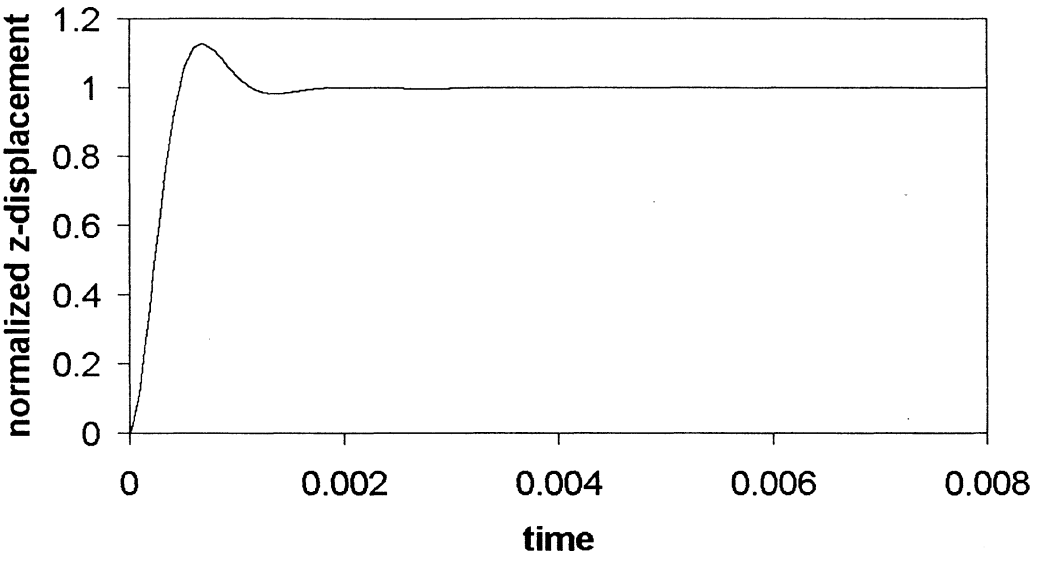

Figure 6.6 Transverse deflection of damped beam without hourglass subcycling

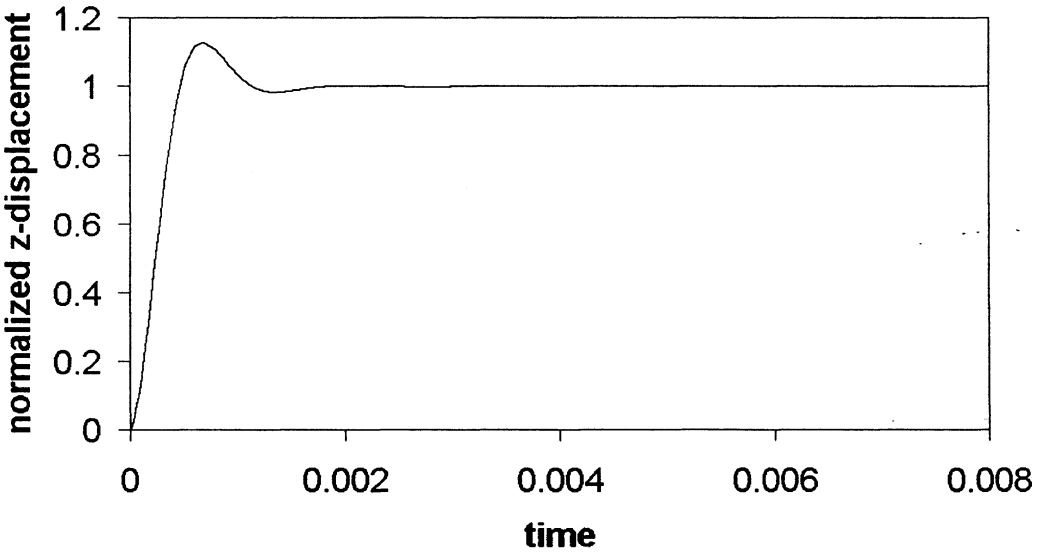

Figure 6.7 Transverse deflection of damped beam with hourglass subcycling

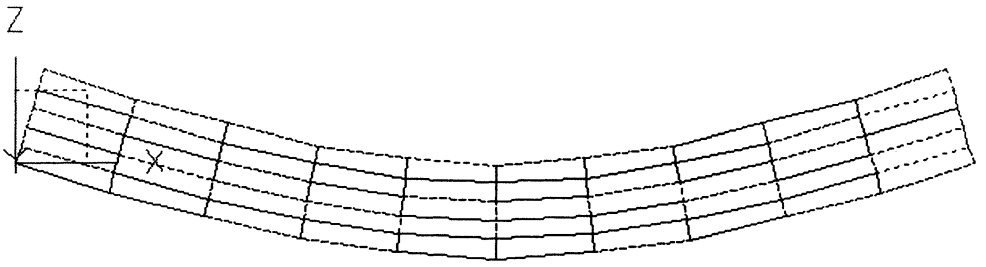

Figure 6.8 Transient deformation without hourglass subcycling when damping applied

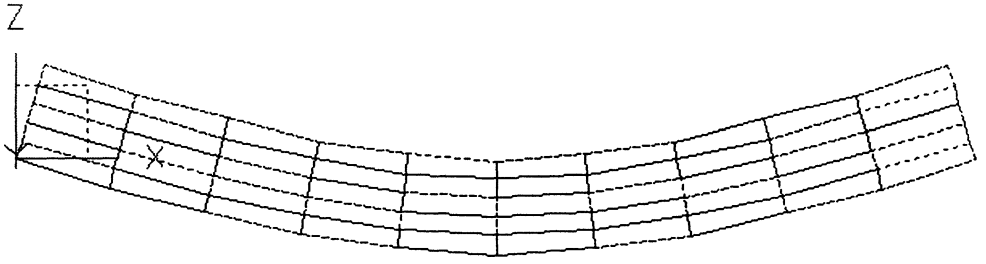

Figure 6.9 Transient deformation with hourglass subcycling when damping applied

In Chapter 5, we found the overall accuracy to be slightly affected by the subcycling approach. However, in above case, the accuracy is surprisingly satisfactory. This is due to an important difference between the finite element model and the spring-mass model. In the finite element model, the hourglass stiffness is not entirely parallel to the primary stiffness. For a rectangular mesh, hourglass force is orthogonal to the single

point quadrature force, though as deformation proceeds a component of hourglass stiffness will be in parallel with the one-point quadrature stiffness [16].

To compare the finite element model and the spring-mass model in a similar way, we change the boundary conditions and load of the finite element model. We let one end be fixed, and apply extension on the other end. Figure 6.10 and Figure 6.11 show the transient deformation without and with hourglass subcycling respectively. The extension of beam without and with hourglass subcycling are shown in Figure 6.12 and Figure 6.13 respectively. The results are normalized with respect to the static displacement of the finite element model.

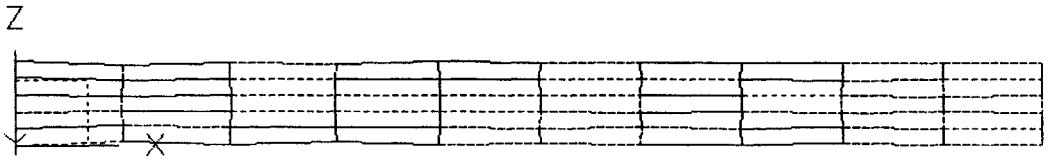

Figure 6.10 Transient deformation without hourglass subcycling

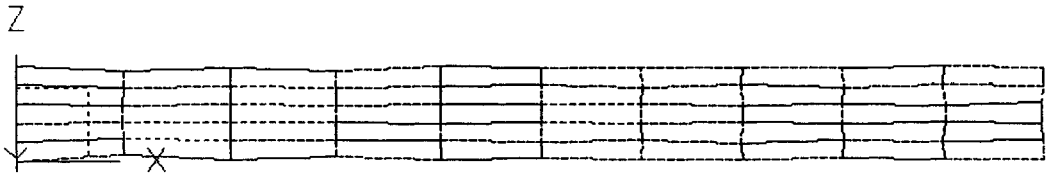

Figure 6.11 Transient deformation with hourglass subcycling

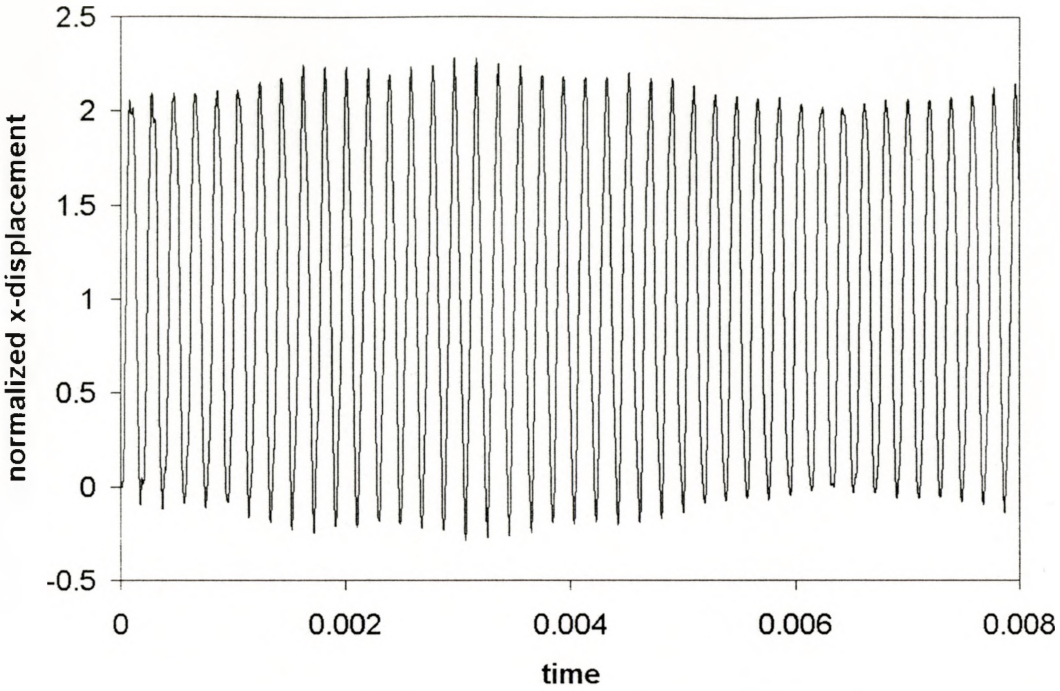

Figure 6.12 Extension of beam without hourglass subcycling

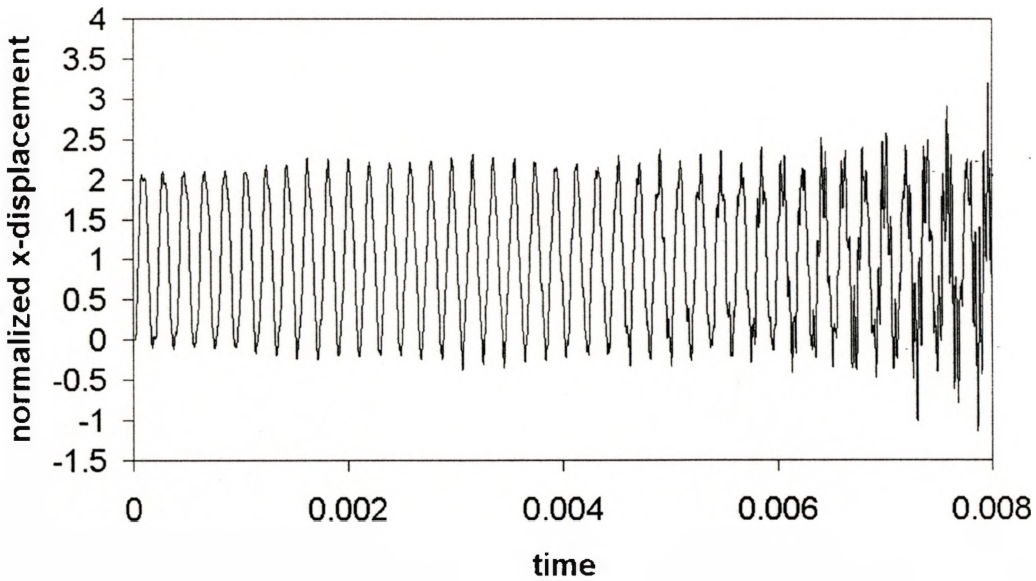

Figure 6.13 Extension of beam with hourglass subcycling

Obviously, when no damping is applied, the hourglass subcycling approach will be unstable. Thus, we add damping to the model. Figure 6.14 and Figure 6.15 show the transient deformation without and with subcycling.

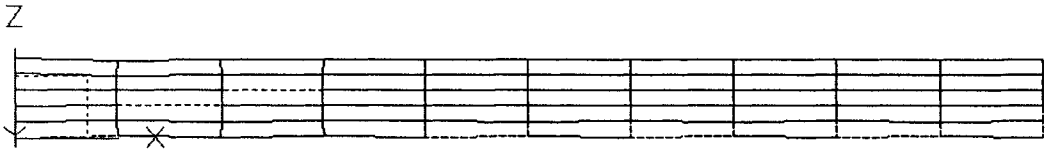

Figure 6.14 Transient deformation without subcycling when damping applied

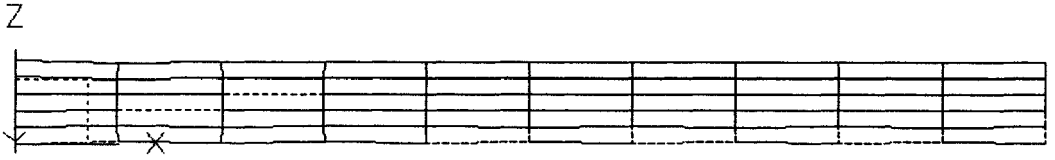

Figure 6.15 Transient deformation with subcycling when damping applied

The extension for normal approach and subcycled approach are shown in Figure 6.16 and Figure 6.17 respectively. Comparing the two results from different approaches, we find that both stability and accuracy are achieved when damping is applied to the model. Therefore, in transient problems, damping can effectively restore the stability of the subcycled approach, and satisfactory accuracy can be achieved as long as the system is stable.

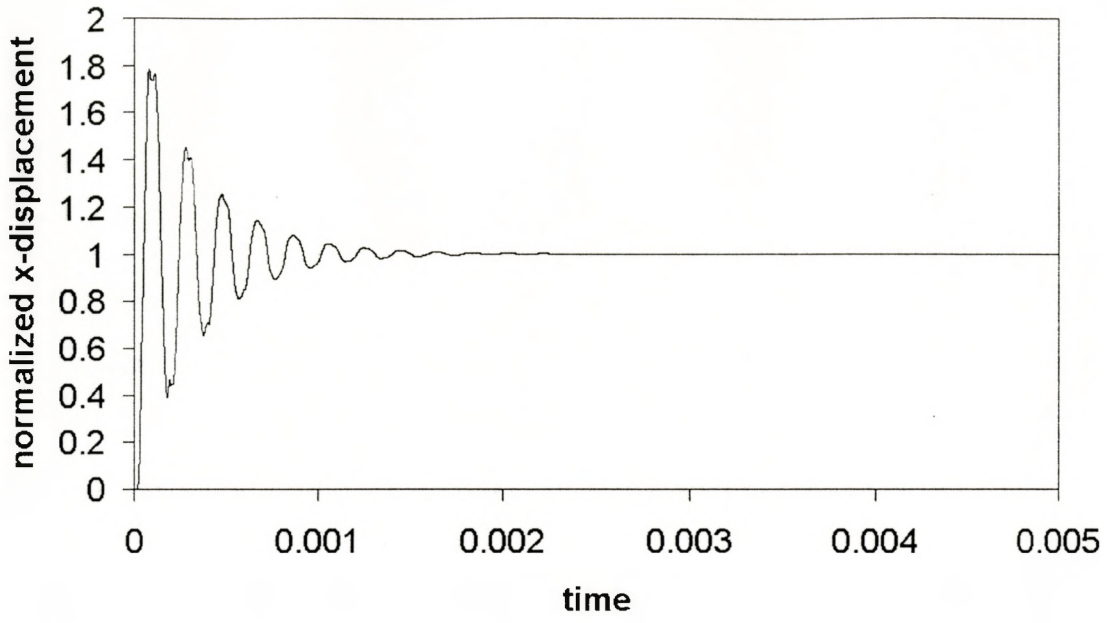

Figure 6.16 Extension of beam without subcycling when damping applied

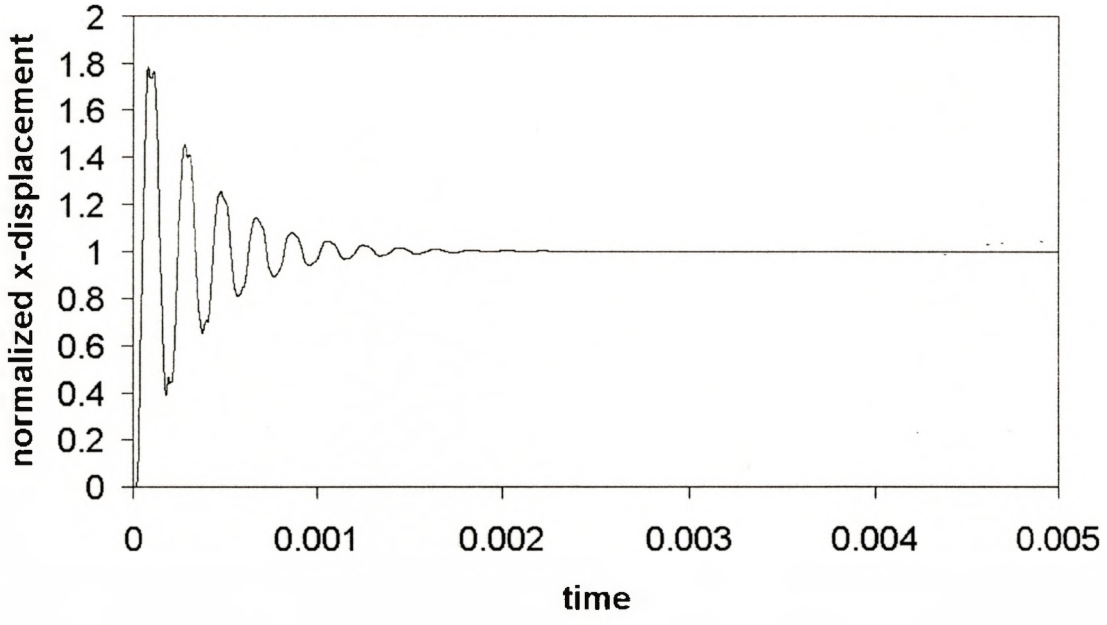

Figure 6.17 Extension of beam with subcycling when damping applied

6.3 Static Solution with Dynamic Relaxation

Using damping to stabilize the subcycling is somewhat limited, because damping usually affects the response. However, we can obtain static solutions with the Dynamic Relaxation method, which is implemented in the H3DMAP code with the subcycling scheme. In the simply supported beam model with a central transverse load, no instability is found in the method, and the equilibrium is reached through a smooth, critically damped approach. Figure 6.18 and Figure 6.19 show the deformed geometry for dynamic relaxation without and with hourglass subcycling respectively.

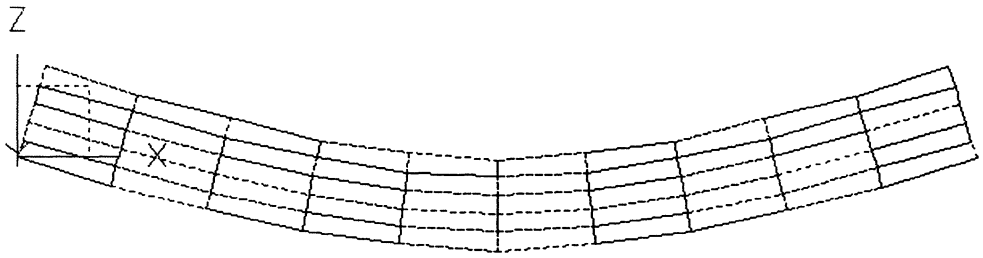

Figure 6.18 Static response, dynamic relaxation without hourglass subcycling

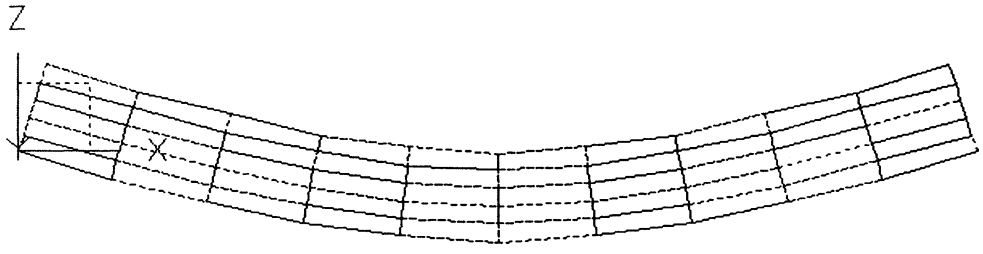

Figure 6.19 Static response, dynamic relaxation with hourglass subcycling

iteration(x1000)

Figure 6.20 Bending deflection history for DR without hourglass subcycling

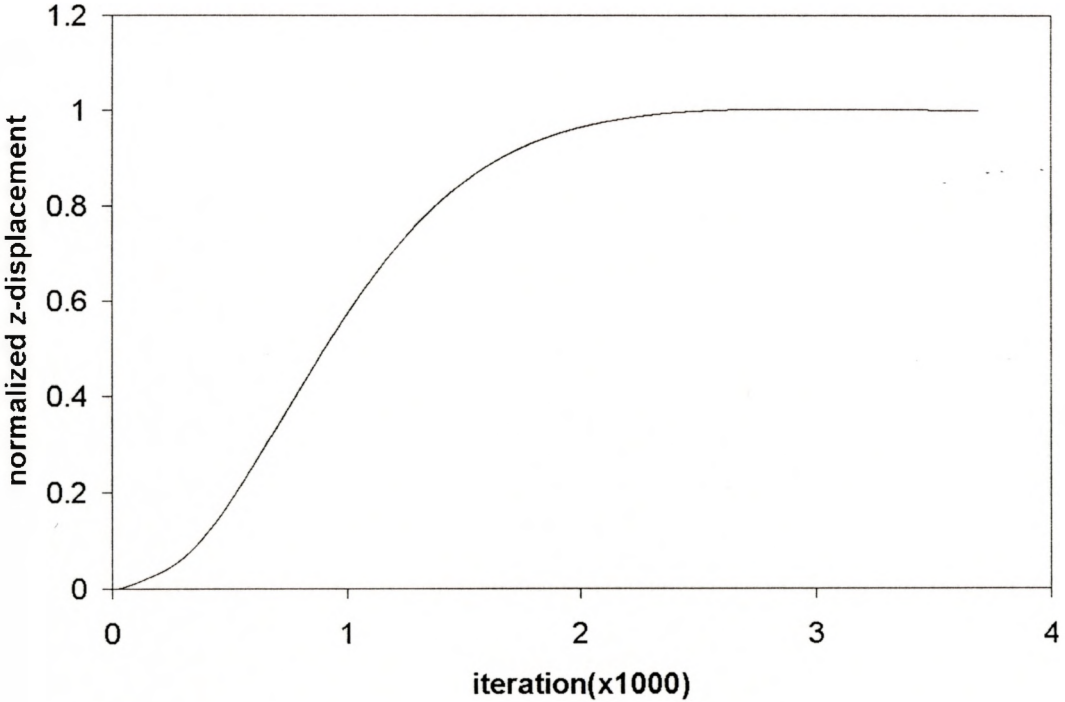

Figure 6.21 Bending deflection history for DR with hourglass subcycling

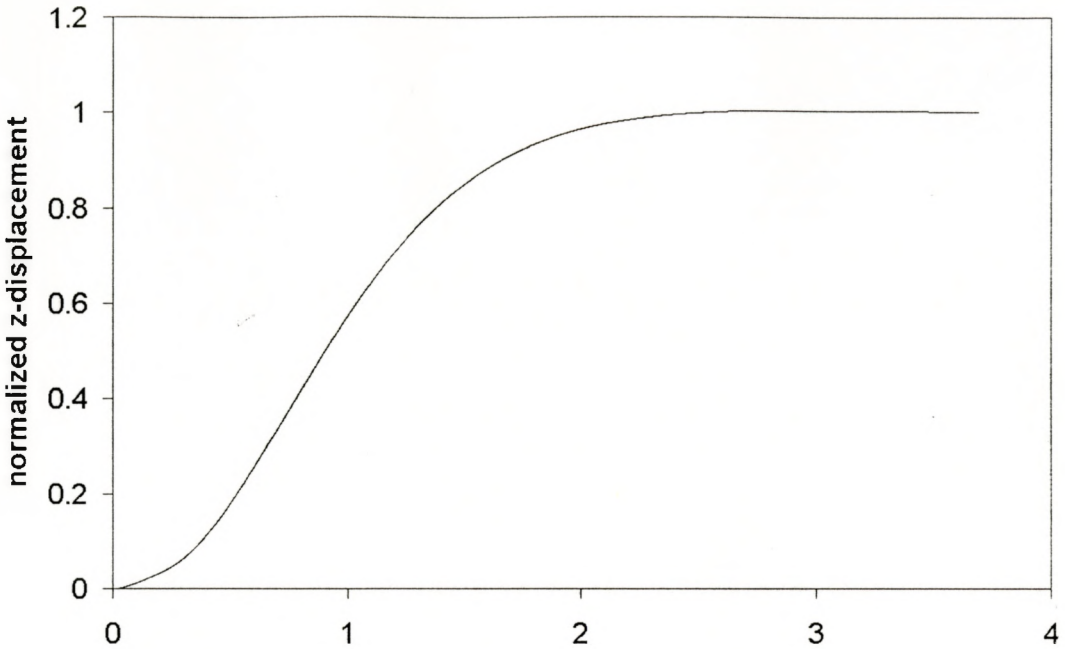
normalized z-displacement
1.2
1
0.8
0.6
0.4
0.2
0
0
1
2
3
4

The deflection history for dynamic relaxation without and with hourglass subcycling is shown in Figure 6.20 and Figure 6.21 respectively. Comparing the two figures, we find the accuracy of the subcycled approach is satisfactory. In addition, when we compare the result of dynamic relaxation with that of transient problems (Figure 6.6 and Figure 6.7), it is found that only the path to the equilibrium is affected.

Then we study the model with one end fixed and pulling force applied to the other end. Figure 6.22 and Figure 6.23 show the static response for dynamic relaxation without and with hourglass subcycling respectively.

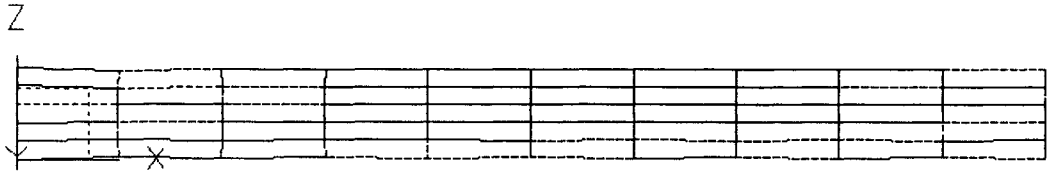

Figure 6.22 Static response in tension, dynamic relaxation without hourglass subcycling

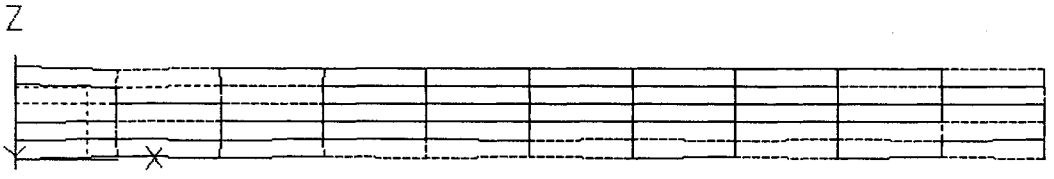

Figure 6.23 Static response in tension, dynamic relaxation with hourglass subcycling

iteration(x1000)

Figure 6.24 Deflection history in tension for DR without hourglass subcycling

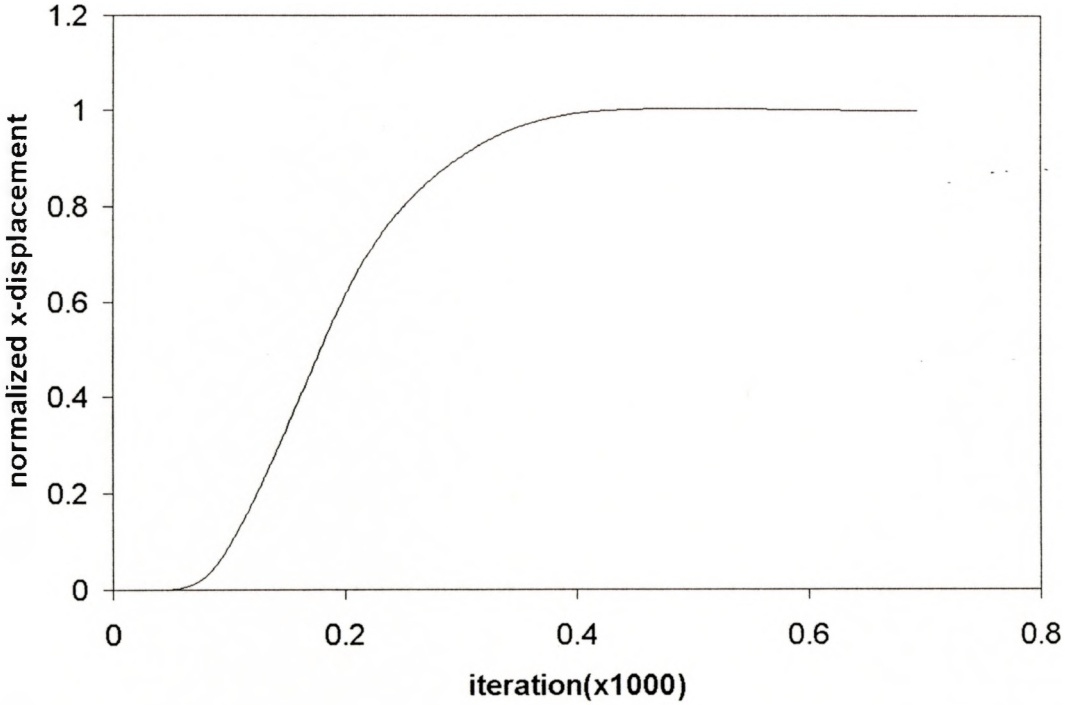

Figure 6.25 Deflection history in tension for DR with hourglass subcycling

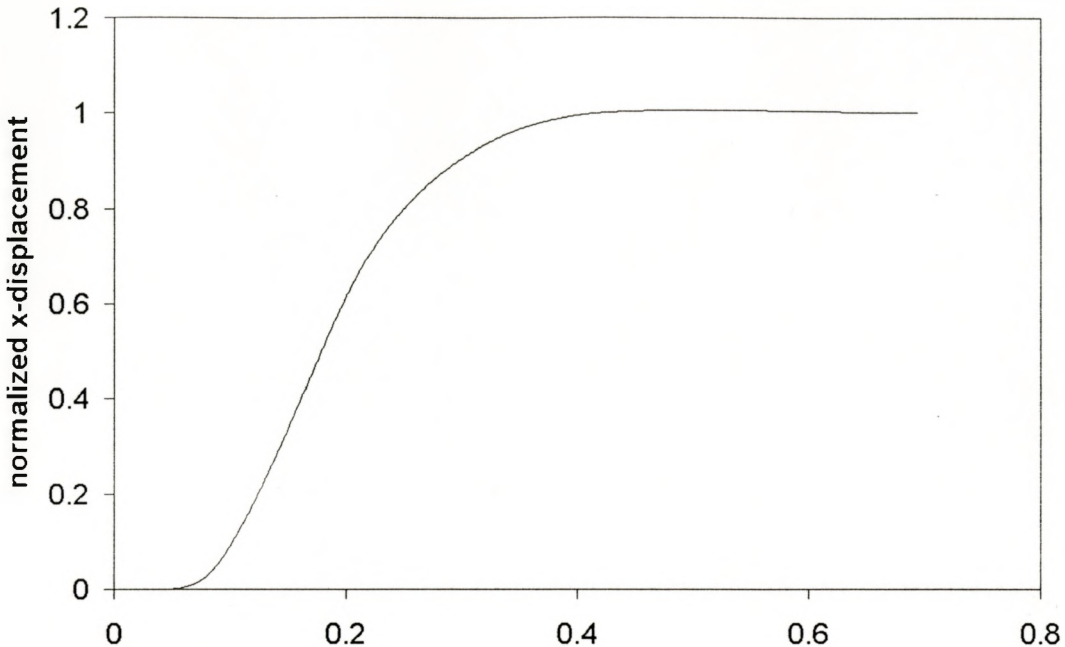
normalized x-displacement
1.2
1
0.8
0.6
0.4
0.2
0
0
0.2
0.4
0.6
0.8

Figure 6.24 and Figure 6.25 demonstrate that in dynamic relaxation the subcycled approach is stable and the accuracy is satisfactory since the results agree to within four significant digits. Comparing the transient response and static solution with dynamic relaxation, the final results are nearly the same and only the paths to the equilibrium are different.

To test the subcycling approach in dynamic relaxation problems with some extreme conditions, we change the load of the simply supported beam model from balanced two loads to only one load on one node. This is a very unfavorable boundary condition even for the usual central difference operator. The load on one node will cause the beam to twist and bend simultaneously, and four hourglass modes can occur in such a condition while only one will occur when the loads are balanced. We want to see how the subcycling approach will response to such a bad loading.

First, we let the penalty factor applied to the hourglass control to be 0.01 as it is in original two-loading model. The result is bad for usual central difference operator as shown in Figure 6.26. The unstable deformations appear to be mainly hourglass modes. Not surprisingly, it is even worse for the subcycling approach as it goes completely unstable.

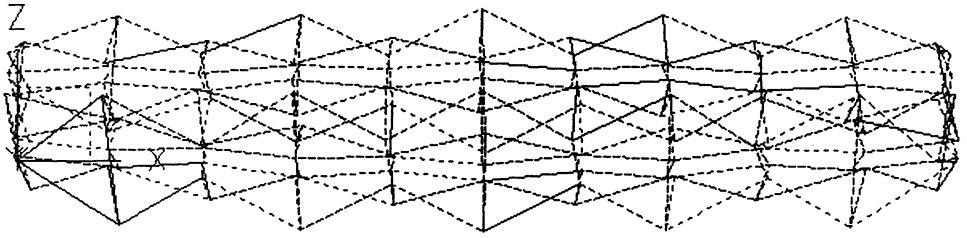

Figure 6.26 Static response, dynamic relaxation without hourglass subcycling

The usual central difference operator appears unstable mainly because the hourglass stiffness is too small to control the hourglass modes. Thus, the penalty factor is adjusted to be 0.1 (a more typical value in practice). Much better results are obtained with both usual central difference operator and the subcycling approach after the change. Figure 6.27 and Figure 6.28 show the static response for usual central difference operator and the subcycling approach respectively.

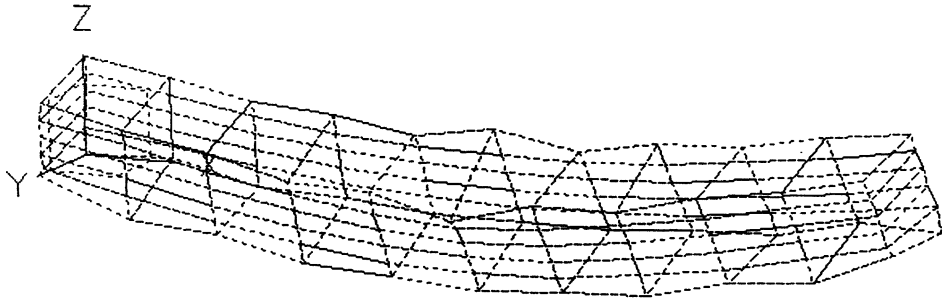

Figure 6.27 Static response, dynamic relaxation without hourglass subcycling

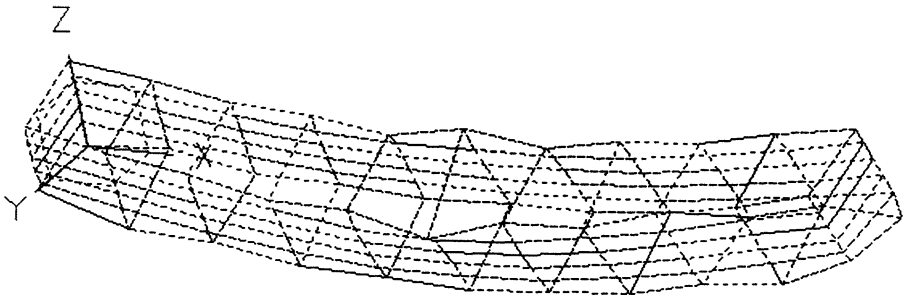

Figure 6.28 Static response, dynamic relaxation with hourglass subcycling

Note that in Figure 6.27 and Figure 6.28, the static responses are shown in a magnified way. The transverse deflections are shown in Figure 6.29 and Figure 6.30 for usual central difference operator and the subcycling approach respectively. The results are normalized with respect to the final displacement of the usual central difference model. The figures demonstrate that when we increase the penalty factory for hourglass control, satisfactory stability and accuracy can be achieved with the subcycling approach.

We can further our study on the model by increasing the penalty factor for hourglass control to 1. This effectively restores full integration for rectangular elements. Figure 6.31 and Figure 6.32 show the static response for usual central difference operator and the subcycling approach respectively when the penalty factor is 1.

iteration(x1000)

Figure 6.29 Deflection history for DR without hourglass subcycling

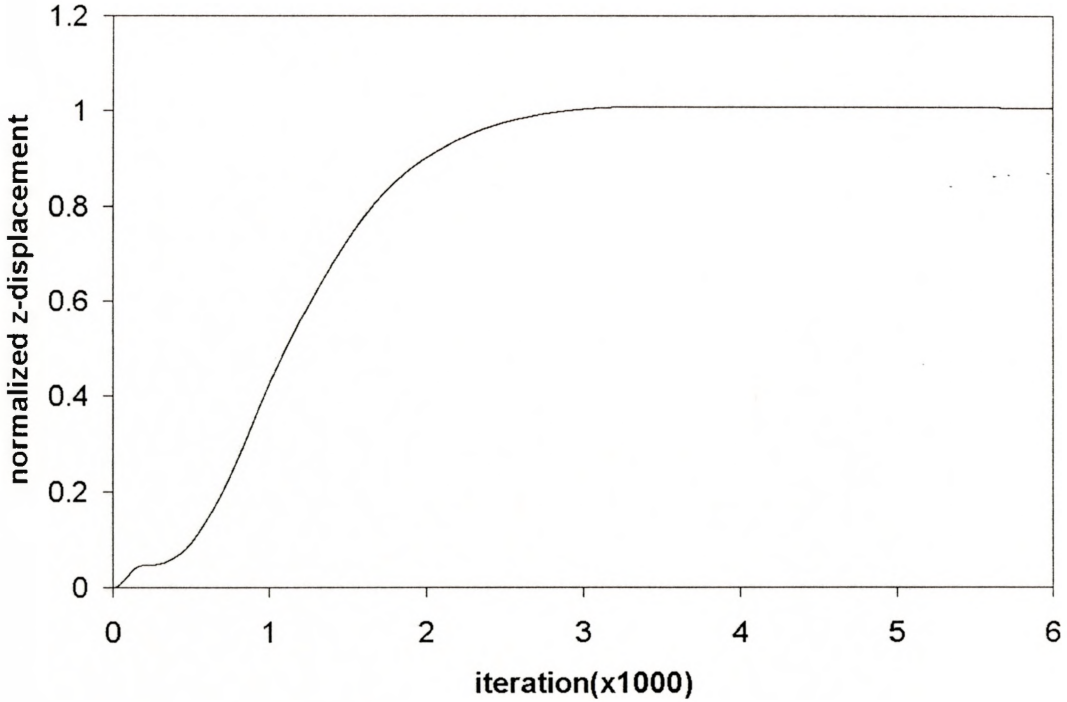

Figure 6.30 Deflection history for DR with hourglass subcycling

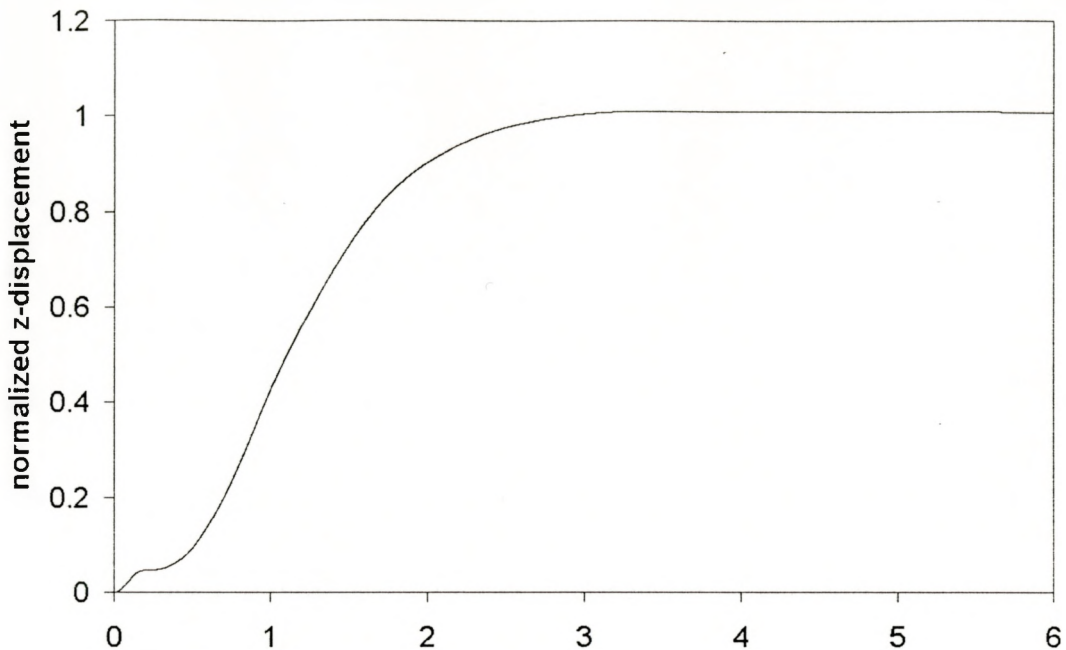
normalized z-displacement
1.2
1
0.8
0.6
0.4
0.2
0
0
1
2
3
4
5
6

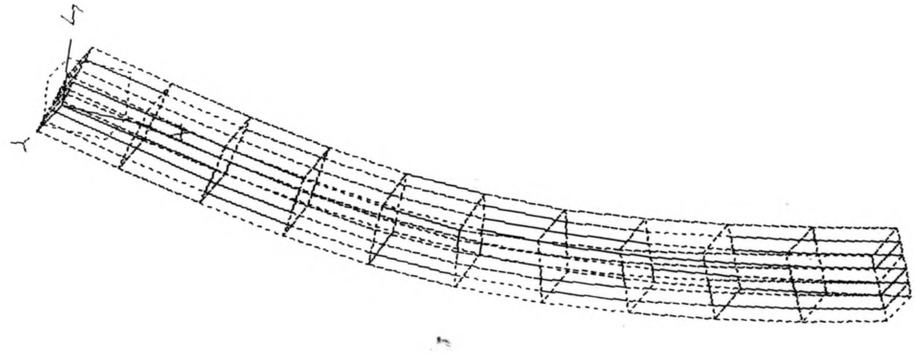

Figure 6.31 Static response, dynamic relaxation without hourglass subcycling

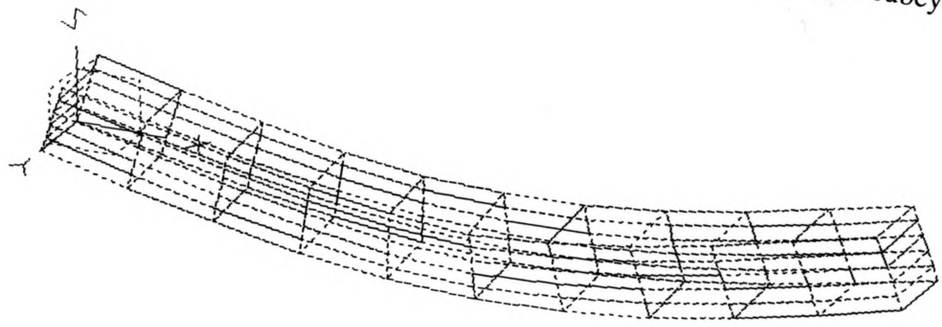

Figure 6.32 Static response, dynamic relaxation with hourglass subcycling

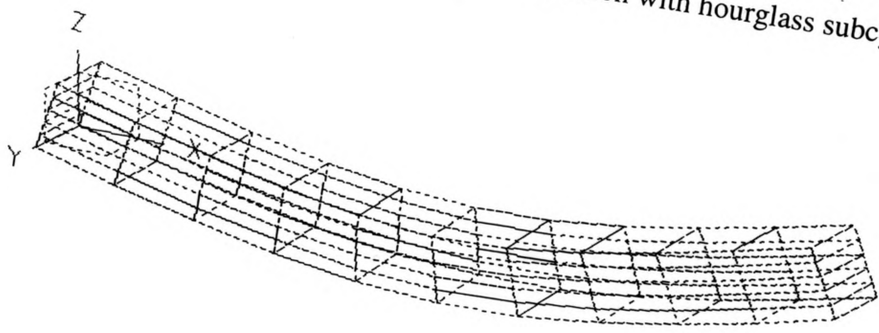

Figure 6.33 Static response generated by I-DEAS

Obviously, stability is greatly improved when we change the penalty factor from 0.1 to 1. The response generated by the subcycling approach is satisfactory when compared to the static solution (Figure 6.33) generated by I-DEAS, which represents a true full integration method. Therefore, in dynamic relaxation problems, as long as the hourglass control is sufficient, the subcycling approach works very well even when the boundary conditions are extremely bad.

6.4 Discussion

For finite element models, in transient problems, the subcycling approach may introduce instability. However, stability can be restored by adding damping to the system. In addition, the overall accuracy is satisfactory as long as the stability is ensured. In dynamic relaxation problems, both stability and accuracy can be achieved. Therefore, the subcycling approach can be applied to a wide variety of problems where damping can be applied.

CHAPTER 7

Discussion and Conclusions

7.1 Discussion

The subcycling approach may only be acceptable where damping can be applied, but the efficiency possible is well worthwhile in many cases. Typically, the evaluation of the hourglass forces accounts for 60% or more of the total computational effort in a finite element analysis. Updating hourglass forces every other step can cut computation time by about 30% without significantly affecting the accuracy of the solution.

In this paper, only linear elastic problems have been examined, but the intention is also for nonlinear problems. Therefore, many aspects of the method need to be explored further. For example, the dissipation of energy due to plastic deformation could prevent the beating instability. This could be investigated with respect to otherwise undamped transient problems.

Moreover, updating the hourglass force at higher multiples of the time step might provide additional computational efficiency. However, the extent to which it could be practical and how it will affect stability and accuracy are currently unknown for the finite

element formulation. It is recommended that the research on hourglass subcycling be continued for a wider range of problems and possibilities than considered in this study.

7.2 Conclusions

A subcycling approach applied to hourglass control of central difference operator. In the mass-spring model, beating instability imposes a reduced time step. However, damping could effectively restore the usual stable time step. This is also demonstrated by finite element implementation. Thus, for a wide variety of problems where damping can be used, the method is highly effective in improving computational efficiency without seriously affect the accuracy of the analysis.

References

[1] Robert D. Cook, David S. Malkus, and Michael E. Plesha, 3rd Ed., Concepts and Applications of Finite Element Analysis, John Wiley & Sons, Inc., New York, 1989.

[2] Klaus-Jurgen Bathe, Finite Element Procedures in Engineering Analysis, Prentice-Hall, Inc., Englewood Cliffs, New Jersey, 1982.

[3] D. S. Malkus and T. J. R. Hughes, "Mixed finite element methods-reduced and selective integration techniques: a unification of concepts", Comput. Methods Appl. Mech. Eng., 15, 63-81, 1978.

[4] J. C. Nagtegaal, D. M. Parks and J. R. Rice, "On numerical accurate finite element solutions in the fully plastic range", Comput. Methods Appl. Mech. Eng., 4, 153-177, 1974.

[5] G. Maenchen and S. Sack, The TENSOR code, in: B. Alder et al., Methods in Computational Physics, Vol. 3, 181-210, Academic Press, New York, 1964.

[6] T. Belytschko and J. M. Kennedy, "Computer models for subassembly simulation", Nuclear Eng. Design, 49, 17-38, 1978.

[7] D. P. Flanagan and T. Belytschko, "A uniform strain hexahedron and quadrilateral with orthogonal hourglass control", Int. j. numer. Methods eng., 17, 679-706, 1981.

[8] T. Belytschko, J. S.-J. Ong, W. K. Liu and J. M. Kennedy, "Hourglass control in linear and nonlinear problems", Comput. Methods Appl. Mech. Eng., 43, 251-276, 1984.

[9] W. K. Liu, J. S.-J. Ong and R. A. Uras, "Finite element stabilization matrices—a unification approach", Comput. Methods Appl. Mech. Eng. 53, 13-46, 1985.

[10] W. K. Liu, T. Belytschko, J. S. J. Ong and S. E. Law, "Use of stabilization matrices in nonlinear analysis", Eng. Comput., 2, 47-55, 1985.

[11] D. R. Metzger and R. G. Sauve, "Three dimensional hourglass stabilization for one point quadrature finite elements", Design Analysis, Robust Methods and Stress Classification, ASME PVP 265, 1993.

[12] B. C. Koh and N. Kikuchi, "New improved hourglass control for bilinear and trilinear elements in anisotropic linear elasticity", Comput. Methods Appl. Mech. Eng. 65, 1-46, 1987.

[13] W. K. Liu, H. Chang, J. S. Chen and T. Belytschko, "Arbitrary Lagrangian-Eulerian petrov—Galerkin finite elements for nonlinear continua", Comput. Methods Appl. Mech. Eng., 68, 59-310, 1988.

[14] T. Belytschko and L. P. Bindeman, "Assumed strain stabilization of the 4-node quadrilateral with 1-point quadrature for nonlinear problems", Comput. Methods Appl. Mech. Eng. 88, 311-340, 1991.

[15] T. Belytschko and L. P. Bindeman, "Assumed strain stabilization of the eight node hexahedral element", Comput. Methods Appl. Mech. Eng. 105, 225-260, 1993.

[16] D. R. Metzger, "Subcycled hourglass control for explicit time integration of finite elements", PVP-Vol. 400, Emerging Technologies: Risk Assessment, Computational Mechanics, and Advanced Engineering Topics, F. L. Cho, Ed; pp. 223-229, 2000.

[17] J. O. Hallquist, "LS-DYNA Theoretical Manual", Lawrence Live-more Software Corporation, 1998.

[18] T. Belytschko, H.-J. Yen and R. Mullen, "Mixed methods for time integration", Computer Methods in Applied Mechanics and Engineering, Vol. 17/18, pp. 259-275, 1979.

[19] A. S. Day, "An introduction to dynamic relaxation", Engineer, 219, 218-221, 1965.

[20] J. R. H. Otter, E. Cassel and R. E. Hobbs, "Dynamic Relaxation", *Proc. Inst. Civ. Engrs*, 35, 633-656, 1966.

[21] J. S. Brew and D. M. Brotten, "Non-linear structural analysis by dynamic relaxation", International Journal for Numerical Methods in Engineering, Vol. 3, pp. 436-483, 1971.

[22] A. Pica and E. Hinton, "Transient and pseudo-transient analysis of Mindlin plates", International Journal for Numerical Methods in Engineering, Vol. 15, pp. 189-208, 1980.

[23] M. Papadrakakis, "A method for the automatic evaluation of dynamic relaxation parameters", Computer Methods in Applied Mechanics and Engineering, Vol. 25, pp. 35-48, 1981.

[24] P. Underwood, "Dynamic relaxation", Computational Methods for Transient Analysis, eds., T. Belytschko and T. J. R. Hughes, North Holland, pp. 245-265, 1983.

[25] D. R. Oakley and N. F. Jr. Knight, "Non-linear structural response using adaptive dynamic relaxation on a massively parallel processor system", International Journal for Numerical Methods in Engineering, Vol. 39, pp. 235-259, 1996.

[26] R. G. Sauve and D. R. Metzger, "Advances in dynamic relaxation techniques for nonlinear finite element analysis", Journal of Pressure Vessel Technology, Vol. 117, pp. 170-176, 1995.

[27] N. M. Newmark, "A method of computation for structural dynamics," *J. Engng. Mech. Div., Proc. ASCE*, Vol. 85, No. EM3, 1959, pp. 67-94.

[28] J. C. Houbolt, "A recurrence matrix solution for the dynamic response of elastic aircraft," *J. Aero. Sci.*, Vol. 17, No. 9, 1950, pp. 540-550.

[29] E. L. Wilson, "A computer program for the dynamic stress analysis of underground structures," *SESM Report No. 68-1*, Division of Structural Engineering and Structural Mechanics, University of California, Berkeley, 1968.

[30] R. G. Sauve, "H3DMAP version 6- a general three–dimensional finite element computer code for linear and nonlinear analysis of structures", Ontario Power Technologies Report No. A-NSG-96-120, Rev. 1, 1999.